HHS Public Access

Author manuscript

Cell. Author manuscript; available in PMC 2022 March 04.

Published in final edited form as:

Cell. 2021 March 04; 184(5): 1214–1231.e16. doi:10.1016/j.cell.2021.01.051.

Enteric helminth coinfection enhances host susceptibility to neurotropic flaviviruses via a tuft cell-IL-4 receptor signaling axis

Pritesh Desai[1], **Hana Janova**[2], **James P. White**[1], **Glennys V. Reynoso**[7], **Heather D. Hickman**[7], **Megan T. Baldridge**[1,3], **Joseph F. Urban Jr.**[6], **Thaddeus S. Stappenbeck**[5], **Larissa B. Thackray**[1], **Michael S. Diamond**[1,2,3,4,#,¶]

[1]Department of Medicine, Washington University School of Medicine, Saint Louis, MO 63110, USA.

[2]Department of Pathology & Immunology, Washington University School of Medicine, Saint Louis, MO 63110, USA.

[3]Department of Molecular Microbiology, Washington University School of Medicine, Saint Louis, MO 63110, USA.

[4]The Andrew M. and Jane M. Bursky Center for Human Immunology and Immunotherapy Programs, Washington University School of Medicine, Saint Louis, MO 63110, USA.

[5]Department of Inflammation and Immunity, Cleveland Clinic, Cleveland, OH 44195, USA.

[6]US Department of Agriculture, Agricultural Research Services, Beltsville Human Nutrition Research Center, Diet, Genomics, and Immunology Laboratory, and Beltsville Agricultural Research Center, Animal Parasitic Diseases Laboratory, Beltsville, MD 20705-2350, USA.

[7]Viral Immunity and Pathogenesis Unit, Laboratory of Clinical Microbiology and Immunology, National Institute of Allergy and Infectious Diseases, NIH, Bethesda, MD 20892, USA

SUMMARY

Although enteric helminth infections modulate immunity to mucosal pathogens, their effects on systemic microbes remain less established. Here, we observe increased mortality in mice coinfected with the enteric helminth *Heligmosomoides polygyrus bakeri* (Hpb) and West Nile

[#]Address correspondence to: Michael S. Diamond, M.D. Ph.D., diamond@wusm.wustl.edu, 314 362-2842.
[¶]Lead Contact: Michael S. Diamond, M.D. Ph.D.

AUTHOR CONTRIBUTIONS

P.D. and M.S.D. designed experiments. P.D., H.J., and J.P.W. performed the WNV and GI tract experiments and analyzed data. G.V.R. and H.D.H. performed and analyzed spleen immunofluorescence imaging studies. J.F.U., M.T.B, T.S.S. and L.B.T. provided critical reagents and experimental advice. P.D. and M.S.D. wrote the initial draft of the manuscript, with all other authors contributing to editing into the final form.

DECLARATION OF INTERESTS

M.S.D. is a consultant for Inbios, Vir Biotechnology, NGM Biopharmaceuticals, and the Carnival Corporation, and on the Scientific Advisory Boards of Moderna and Immunome. The Diamond laboratory has received unrelated funding under sponsored research agreements from Moderna, Vir Biotechnology, and Emergent BioSolutions.

virus (WNV). This enhanced susceptibility is associated with altered gut morphology and transit, translocation of commensal bacteria, impaired WNV-specific T cell responses, and increased virus infection in the gastrointestinal tract and central nervous system. These outcomes were due to type 2 immune skewing, as coinfection in *Stat6*$^{-/-}$ mice rescues mortality, treatment of helminth-free WNV-infected mice with IL-4 mirrors coinfection, and IL-4 receptor signaling in intestinal epithelial cells mediates the susceptibility phenotypes. Moreover, tuft cell-deficient mice show improved outcomes with coinfection, whereas treatment of helminth-free mice with tuft cell-derived cytokine IL-25 or ligand succinate worsens WNV disease. Thus, helminth activation of tuft cell-IL-4-receptor circuits in the gut exacerbates infection and disease of a neurotropic flavivirus.

Graphical Abstract

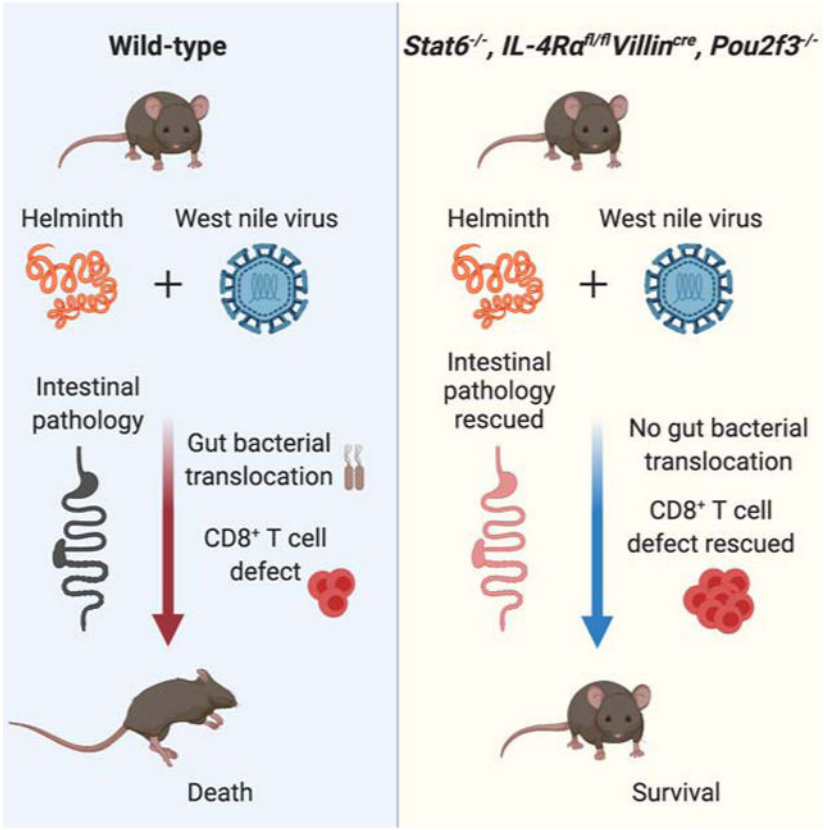

INTRODUCTION

More than two billion people in the world are infected with helminths (Hotez et al., 2008). Millions of years of coevolution has enabled helminths to evade mammalian host responses and persist without causing severe disease in most individuals (Allen and Maizels, 2011). A benefit of this commensal-like relationship to the mammalian host may be a tempered immune response, since eradication of helminths correlates with higher prevalence of dysregulated immune disorders such as asthma, allergy, and autoimmunity (Cheng and Locksley, 2014; Loke and Lim, 2015). Nonetheless, helminth-endemic areas also have

higher incidences of some systemic infections including HIV, malaria, and *Mycobacterium tuberculosis* (*Mtb*), raising the possibility that helminth infection can impair host immunity against certain pathogens (Salgame et al., 2013). Experimental evidence examining the influence of helminths on the host immune responses against viruses are few, and these studies have reported discordant findings.

Coinfection with enteric helminths may benefit the host response against respiratory viral infections (Furze et al., 2006; McFarlane et al., 2017; Scheer et al., 2014). Coinfection of mice with *Trichinella spiralis* and influenza A virus resulted in improved clinical outcome (Furze et al., 2006), and the enteric helminth *Heligmosomoides polygyrus bakeri* (Hpb) protected mice against respiratory syncytial virus (McFarlane et al., 2017). In contrast, coinfection with helminths promoted viral replication after enteric infection with murine norovirus (MNoV) (Osborne et al., 2014), and this was attributed to impaired virus-specific $CD8^+$ T cells resulting from IL-4-mediated differentiation of macrophages and increased tuft cells numbers (Osborne et al., 2014; Wilen et al., 2018). While another study also implicated IL-4-induced macrophages in reactivation of gammaherpesvirus infection (Reese et al., 2014), others have suggested that IL-4 signaling can boost virus-specific $CD8^+$ T cell responses and inhibit gammaherpesvirus infection during helminth coinfection (Rolot et al., 2018). These studies highlight that helminth-virus coinfection can result in different outcomes depending on the virus, the site of infection, and the nature of protective immunity.

Tuft cells initiate type 2 immune responses against enteric helminths and protozoan parasites (Gerbe et al., 2016; Howitt et al., 2016; von Moltke et al., 2016). Upon sensing these organisms, tuft cells produce IL-25, which activates group 2 innate lymphoid cells (ILC2s) in the lamina propria. ILC2s interact with dendritic cell (DC)-primed $CD4^+$ T cells resulting in Th2 cell differentiation (Oliphant et al., 2014). Both ILC2 and Th2 cells produce type 2 cytokines, which signal IL-4Rα expressing intestinal epithelial progenitor cells in the crypts of the small intestine (SI) (Gerbe et al., 2016; von Moltke et al., 2016) and skew their differentiation towards goblet cell and tuft cell lineages. Type 2 cytokines also affect intestinal smooth muscle contractility and stimulate enteric neurons, which together with changes in the intestinal epithelial response, contribute to ‘the weep and sweep response’ that facilitates worm expulsion (Reynolds et al., 2012). While such remodeling of the gastrointestinal (GI) tract prevents worm colonization (Schneider et al., 2018), its effects on other enteric and non-enteric pathogen infections remain less well studied.

Several medically important viruses comprise the Flavivirus genus including Dengue (DENV), Zika (ZIKV), yellow fever (YFV), West Nile (WNV), and tick-borne encephalitis (TBEV) viruses (Daep et al., 2014). These viruses are transmitted principally by arthropod vectors and collectively infect more than 400 million individuals each year (Daep et al., 2014). Among them, WNV is a neurotropic flavivirus that continues to emerge globally. Although in most humans, WNV infection is asymptomatic, ~10-30% of individuals develop a febrile illness or neurological disease (Daep et al., 2014). Although some genetic factors (*e.g.*, *CCR5Δ32* and *OAS1* alleles) are linked to susceptibility (Bigham et al., 2011; Lindsey et al., 2012), these do not explain the majority of severe WNV cases .

In addition to targeting neurons in the brain and spinal cord, WNV replicates in enteric neurons of the myenteric plexus, where infection results in neuronal injury and GI tract dysmotility (White et al., 2018). Perturbations of the gut microbiota can modulate host resistance and susceptibility to flavivirus infection (Thackray et al., 2018). It remains uncertain whether other factors, such as coinfection with helminths, could affect disease severity caused by WNV or other flaviviruses.

Here, we explored whether coinfection with the non-migrating enteric helminth Hpb modulates flavivirus-induced disease. Hpb is an endogenous mouse helminth that is widely used as a model for human intestinal hookworm infection (Bouchery et al., 2017). Upon oral gavage with the infective L3 larval stage, Hpb larvae penetrate the SI submucosa and undergo two developmental molts before emerging into the gut lumen as mature adults. The adult parasites coil around the intestinal villi, feed on the intestinal epithelium, mate, and produce eggs that are excreted in the feces. Although Hpb infection elicits a robust type 2 immune response that reduces the worm burden, it does not clear helminths, enabling persistent infection in C57BL/6 mice (Reynolds et al., 2012).

We found that mice coinfected with Hpb and WNV had higher mortality rates compared to WNV- or Hpb-only infected mice, and this phenotype correlated with higher viral burden in coinfected mice. Coinfection in mice resulted in macroscopic changes to the SI, gut motility defects, and neuronal network changes. Histopathological analyses revealed alterations in the SI mucosa including crypt hyperplasia, villus blunting, and increased enterocyte turnover. These defects were associated with translocation of gut bacteria into the blood to the spleen, which resulted in the collapse of antiviral $CD8^+$ T cell responses. Notably, Hpb and WNV coinfection did not cause these disease phenotypes in *Stat6*$^{-/-}$ mice. Conversely, administration of IL-4-anti-IL-4 complexes (IL-4c) to helminth-free WNV-infected mice resulted in the same deleterious GI tract and systemic immune phenotypes as observed in coinfected mice. A lack of IL-4 receptor (IL-4Rα) expression on myeloid or hematopoietic cells did not alter WNV or GI tract disease in the context of Hpb coinfection, whereas a loss of IL-4Rα expression on intestinal epithelial cells mitigated disease and improved survival. Finally, mice lacking tuft cells, showed improved survival, intact WNV-specific $CD8^+$ T cell responses, and an absence of gut pathology in the context of coinfection. Collectively, these results indicate that systemic infection with WNV in the presence of enteric helminth coinfection activates a tuft cell-type 2 immunity-intestinal epithelial cell circuit that damages the GI epithelial barrier, which results in translocation of gut bacteria, altered splenic architecture, and loss of virus-specific $CD8^+$ T cells. Ultimately, this leads to enhanced WNV infection in the central nervous system (CNS) and increased mortality in mice. As a similar pattern was observed with ZIKV or Powassan (POWV) coinfection, enteric helminths may enhance the disease severity of multiple neurotropic flaviviruses.

RESULTS

Coinfection with the enteric helminth Hpb exacerbates WNV disease severity.

To assess the impact of enteric helminth infection on WNV pathogenesis, we gavaged 9-week old C57BL/6J mice with infective third-stage Hpb larvae (L3), and 12 days later inoculated them subcutaneously with WNV in the footpad (Fig 1A). Day 12 marks the onset

of patency, when adult forms of Hpb emerge and mate in the intestinal lumen resulting in egg production. Coinfected mice were compared to mice infected with Hpb or WNV alone. Infection with Hpb alone had no adverse effect on survival or body weight, whereas infection with WNV alone resulted in an 86% survival rate and modest reductions in body weight (Fig 1B-C). In contrast, only 28% of coinfected mice survived by 20 days post-infection (dpi). Coinfected mice also displayed greater weight loss than mice infected with WNV or Hpb alone. Helminth infection also increased the susceptibility of mice to other neurotropic flaviviruses, including POWV and ZIKV (Fig S1A-B).

To begin to determine the cause of the greater mortality in coinfected mice, we examined the kinetics of WNV infection. Viral RNA was detected in the draining lymph nodes (DLN) of the foot as early as 1 dpi, and was sustained until 10 dpi in both coinfected and WNV-only infected mice (Fig 1D). Viral RNA levels also were equivalent in the spleens of coinfected and WNV-only infected group at all time points (Fig 1E). Although, we did not detect early virus entry into the CNS, at 10 dpi, higher viral RNA levels were present in the brain and the spinal cord of coinfected than WNV-only infected mice (Fig 1F-G). Since WNV also has a tropism for the GI tract (White et al., 2018), we measured infection at this site. We observed higher viral titers at 10 dpi in the mesenteric lymph node (MLN), proximal SI, distal SI, and colon of coinfected (Fig 1H-K) than WNV-only infected (Fig 1H) mice. These results show that Hpb infection affects WNV burden at later phases in the CNS and the GI tract, suggesting an effect on immune clearance. We also evaluated whether WNV reciprocally influenced the Hpb lifecycle by measuring adult worm egg production in feces of mice. We observed no significant differences in egg burden at 3 and 6 dpi between coinfected or Hpb-only infected mice (15 and 18 days, respectively, post-inoculation with Hpb L3) (Fig S1C-D).

To corroborate the relationship between helminth infection and WNV infection outcome, we treated mice with pyrantel pamoate, an anti-helminthic drug. When Hpb-infected mice were gavaged with pyrantel pamoate prior to WNV infection, the egg burden was reduced to undetectable levels (Fig S1E-F). As anti-helminthic treatment also abolished the enhanced mortality observed during Hpb and WNV coinfection (Fig S1G), helminth colonization is necessary for enhanced susceptibility to WNV infection.

Hpb and WNV coinfection causes changes in the GI tract that impact intestinal motility.

Systemic infection of C57BL/6 mice with highly pathogenic WNV strains (New York, 1999) results in dilation of intestinal segments and altered GI tract motility (White et al., 2018). We observed fewer macroscopic changes to the SI at 10 dpi after inoculation with a WNV strain (New York 2000) that is less pathogenic in mice (Fig 2A). In contrast, mice coinfected with Hpb and WNV New York 2000 showed marked changes in the GI tract including dilation of the proximal segments of the SI, blackening of the bowel, and tissue friability. Moreover, the distal section of the SI and the entire colon appeared void of luminal contents, a sign of gut dysmotility (Fig 2A). We measured intestinal transit times of a carmine dye in animals that were uninfected, singly-infected (Hpb or WNV), or coinfected. At 2 dpi, there were no differences between the groups (Fig 2B). By 6 dpi, transit delays were apparent in a subset of WNV-only and coinfected mice (Fig 2C). By 10 dpi, approximately 70% of coinfected

mice showed marked delays (> 6h) in GI motility whereas this extent of dysmotility was observed in ~20% of WNV-only infected mice (Fig 2D).

Hpb enhances WNV infection of enteric neurons.

WNV preferentially infects enteric neurons of the myenteric plexus and sub-mucosal plexus in the GI tract (White et al., 2018). To determine if Hpb coinfection alters the WNV tropism in the GI tract, we co-stained for WNV antigen and Tuj1, a pan-neuronal marker in the SI. We found WNV antigen principally in neuronal cells of the muscularis layer in coinfected mice (Fig S2A), as seen previously (White et al., 2018). To examine this in more detail, we stained whole-mount preparations of the proximal SI muscularis propria and submucosa. We co-stained for WNV antigen and neuronal markers, nNOS and calretinin, that respectively delineate inhibitory and excitatory neurons. Higher levels of WNV antigen were apparent in coinfected than WNV-only infected mice and localized with neuronal ganglia (both nNOS and calretinin) of the myenteric and submucosal plexus (Fig 2E-F, S2B-C). Similar results were observed in the mid SI (Fig 2G). WNV coinfection also affected the enteric neuronal network, as reduced intensity and density of nNOS and calretinin staining was apparent in the myenteric plexus compared to naïve, WNV-only, or Hpb-only infected mice (Fig 2H-J).

Tissue-resident macrophages associate with enteric neuronal ganglia and are implicated in sepsis-induced dysmotility and diabetes-induced gastroparesis (Muller et al., 2020). To examine the effect of coinfection on the macrophage response, we analyzed their distribution in the proximal SI. In naïve mice, macrophages were dispersed and had a stellate morphology, whereas in Hpb-infected mice, they were spindly and occupied more area (Fig S2D). In WNV-infected mice, macrophages were more elongated and accumulated near WNV antigen-positive cells (Fig S2D). These changes in morphology and positioning were more pronounced in coinfected mice. A macrophage response in coinfected mice may occur to limit neuronal loss, as a prior study indicated their importance in preventing bacterial infection-induced neuronal death (Matheis et al., 2020).

Hpb and WNV coinfection causes pathological changes in the intestinal mucosa that enable translocation of commensal bacteria.

We analyzed SI tissue sections for pathological changes during Hpb and WNV coinfection at 10 dpi (corresponding to 22 days after Hpb inoculation). Mice infected with WNV or Hpb alone showed only modest reductions in villus height in the proximal SI (Fig 3A). In contrast, coinfected mice showed a dramatic change in mucosal architecture throughout the proximal SI (Fig 3A). The height of villi in coinfected mice was reduced in comparison with naïve and Hpb or WNV-only infected mice (Fig 3A-B). The villus morphology in coinfected mice showed epithelial cellular crowding and focal tufting (Fig 3A). Shorter villi are commonly associated with diminished epithelial stem/progenitor cell activity (Lee et al., 2009). However, the coinfected mice showed greater crypt depth and epithelial proliferation as measured by the number of M-phase cells, suggesting that cellular turnover in the villi was accelerated (Fig 3A, C, and E). As further evidence of greater epithelial turnover in coinfected mice, we observed increased cell death as judged by TUNEL staining in the proximal SI at 10 dpi (Fig S3C-D). Despite the severity of the mucosal epithelial abnormalities, we did not detect areas of mucosal ulceration or inflammation. The

pathological phenotype in the coinfected mice was greatest in the proximal SI and diminished along the length of the remainder of the SI (Fig S3A-B), which correlates with the localization of Hpb infection (Johnston et al., 2015).

Histological features similar to that seen in coinfected mice have been observed in human pathological conditions and mice with reduced barrier function (Kau et al., 2015; Sivagnanam et al., 2008; Szabo et al., 2019). To evaluate whether structural changes to the SI mucosa associated with coinfection might disrupt the GI tract barrier and allow commensal bacterial translocation, we measured bacteria in the spleen of coinfected mice and compared this to naïve mice or mice infected with WNV or Hpb alone. At 2 dpi, aerobic bacteria did not grow from splenic homogenates (Fig 3F). However, at 6 dpi, we detected low levels of bacteria growing from the splenic homogenates of coinfected mice (Fig 3G), and by 10 dpi, the majority of samples from coinfected mice grew bacteria whereas those from other groups of mice did not (Fig 3H). Analogous results were observed in the blood at 10 dpi (Fig 3I). These effects on barrier permeability were confirmed using an orally-administered FITC-dextran, which showed higher levels of intestinal permeability in coinfected mice than singly-infected mice at 10 dpi (Fig S3E).

Hpb and WNV coinfection compromises WNV-specific CD8$^+$ T cell responses.

Because antiviral CD8$^+$ T cells contribute to clearance of WNV infection (Shrestha and Diamond, 2004), we hypothesized that the viral burden differences we observed at 10 dpi between coinfected mice and WNV-infected mice might be due to effects on T cell responses. To address this question, we measured CD8$^+$ T cell responses in coinfected and WNV-only infected mice using D^b-restricted NS4B tetramers, which recognize WNV-specific CD8$^+$ T cells (Purtha et al., 2007). At 7 dpi, the percentages and numbers of WNV-specific CD8$^+$ T cells in the spleen and the brain were equivalent between the groups (Fig 4A-B). In the MLN, WNV-specific CD8$^+$ T cell numbers were higher in the coinfected group than the WNV-only infected group (Fig 4C). However, at 10 dpi, the percentage and number of WNV-specific CD8$^+$ T cells in the spleen of coinfected mice were markedly reduced compared to WNV-only infected mice (Fig 4D). Similar results were observed in the brain at 10 dpi (Fig 4E) despite the higher viral loads (Fig 1F). However, WNV-specific CD8$^+$ T cells in the MLNs remained comparable between the two groups at 10 dpi (Fig 4F). Thus, although the early WNV-specific CD8$^+$ T cell response is induced normally, there is a decline by 10 dpi in some organs of coinfected mice.

We assessed whether the waning WNV-specific CD8$^+$ T cell response at 10 dpi in coinfected mice was due to effects on proliferation, differentiation, or cell death. At 7 dpi, the expression of Ki67, a cell proliferation marker, was similar between WNV-specific CD8$^+$ T cells of coinfected and WNV-only infected mice (Fig 4G). WNV-specific CD8$^+$ T cells from both groups also expressed similar levels of the T-box transcription factor T-bet, suggesting that differentiation was not altered (Fig 4H). Analogous results were observed in WNV-specific CD8$^+$ T cells from the DLN at 7 dpi (Fig S4A-B). The differentiation of WNV-specific CD8$^+$ T cells into terminal effectors [KLRG1^{hi}CD127^{lo}] and memory precursors [KLRG1^{lo}CD127^{hi}] also was similar between the groups at 7 dpi (Fig 4I). To examine if the reduction in WNV-CD8$^+$ T cell response at 10 dpi was due to altered survival, we stained

cells for annexin V, a marker of cell apoptosis, at 8 dpi. As expected, in naïve mice, most of the $CD8^+$ T cells [90%] were non-apoptotic [Live/dead^{neg}AnnexinV^{neg}] with few in the early [Live/dead^{neg}AnnexinV^{pos}] or late [Live/dead^{pos}AnnexinV^{pos}] stages of apoptosis (Fig 4J). In WNV-only infected mice, virus-specific $CD8^+$ T cells were distributed evenly between non, early, and late apoptotic stages (Fig 4J). This pattern is expected since a proportion of effector $CD8^+$ T cells undergo contraction after WNV clearance (Aguilar-Valenzuela et al., 2018). In coinfected mice, however, a higher percentage of WNV-specific $CD8^+$ T cells were in the late stage of apoptosis and undergoing cell death (Fig 4J). This suggests that the attrition of WNV-specific $CD8^+$ T cells is due in part to impaired survival. When annexin V expression was assessed on bulk $CD8^+$ T cells, major differences were not seen between the two groups (Fig S4C). Thus, the survival defect likely is specific for the antigen-experienced $CD8^+$ T cells in coinfected mice.

To elucidate the basis for enhanced cell death of WNV-specific $CD8^+$ T cells during coinfection, we visualized the organization of the spleen at 7 and 10 dpi by confocal microscopy. Naïve mice showed a clear demarcation of B cell follicles ($B220^+$; purple) and T cell zones ($CD8^+$; green) (Fig 4K). Hpb-infected mice showed cellular infiltration in the T cell zones, as an overlap between DCs and T cells was visible. In comparison, WNV-only and coinfected mice showed minimal co-localization between DCs and $CD8^+$ T cells at the 7-dpi time point (Fig 4K). By 10 dpi, we detected co-localization of DCs and T cells in WNV-only infected mice, but not in coinfected mice (Fig 4L).

To examine whether DCs and other immune cells are impacted by Hpb and WNV coinfection, we quantified their numbers. We observed an ~3.5-fold reduction in number of splenocytes in coinfected compared to WNV-infected mice, and a similar trend was noted for B cells, $CD4^+$ T cell subsets, and $CD8^+$ T cells (Fig S4D-E). Among innate immune cells, greater reductions were observed for natural killer cells than neutrophils, monocytes, eosinophils, or macrophages in coinfected compared to WNV-only infected mice (Fig S4F). DCs in coinfected mice also were reduced compared to WNV-only infected mice (Fig S4F). Thus, the lack of microscopic overlap between DCs and T cells observed in the spleens of coinfected mice may be due to decreases in DC numbers.

We also examined the expression of the stromal cell marker ERTR-7, follicular DC marker CD21/35, and marginal zone macrophage (MZM) marker CD169 in the spleen at 10 dpi. Coinfected mice had reduced ERTR-7 expression, indicating a disruption of splenic architecture (Fig S4G). In contrast, expression of CD169 and accumulation of MZMs was greater in coinfected mice than other groups (Fig S4G). This effect may be a response to the bacteria observed in the spleen of coinfected mice (Fig 3H), since MZMs capture bacteria (Borges da Silva et al., 2015; Perez et al., 2017). Altogether, our experiments suggest that the early cellular immune response (up to 7 dpi) is intact and comparable between the groups. However, later in infection (10 dpi), the splenic architecture of coinfected mice becomes altered, likely due to bacterial invasion, which impacts key immune cell types including DCs and WNV-specific $CD8^+$ T cells that are important for viral clearance (Hildner et al., 2008; Shrestha and Diamond, 2004).

Hpb and WNV coinfection outcomes are rescued in *Stat6*$^{-/-}$ mice.

Infection with enteric helminths induces a Th2 response that depends on signaling by the transcription factor STAT6 (Reynolds et al., 2012; Zhu et al., 2001). As reported previously with other helminths (Urban et al., 1998; Urban et al., 2000), enteric infection of *Stat6*$^{-/-}$ mice with Hpb results in increased parasite egg burden compared to WT mice (Fig S5A) due to impaired Th2 responses in the MLN and spleen (Fig S5B). In comparison, CD25^{+}FoxP3^{+} regulatory CD4^{+} T cell responses in lymphoid tissues are similar in *Stat6*$^{-/-}$ and WT mice (Fig S5C). To determine if type 2 immune responses contribute to the lethality observed after coinfection, we infected WT and *Stat6*$^{-/-}$ mice. All *Stat6*$^{-/-}$ and WT mice survived Hpb infection alone, and most animals also survived WNV infection alone (82% for WT and 79% for *Stat6*$^{-/-}$ mice) (Fig 5A). However, the increased lethality observed during coinfection of WT mice was not observed in *Stat6*$^{-/-}$ mice (13% for WT and 70% survival for *Stat6*$^{-/-}$ mice). When we examined the viral burden in WNV-infected and coinfected *Stat6*$^{-/-}$ mice at 10 dpi, no significant differences were observed in the spleen, brain, spinal cord, and GI tract (Fig 5B). Thus, a deficiency of STAT6 prevents the increase in WNV burden and mortality caused by Hpb coinfection.

We assessed whether a deficiency in STAT6 rescued coinfected mice from the gut abnormalities observed in WT mice. The macroscopic changes associated with coinfection in WT mice (Fig 3A) were absent in *Stat6*$^{-/-}$ mice (Fig 5C). At 10 dpi, many of the coinfected *Stat6*$^{-/-}$ mice did not develop bowel dysmotility, as GI transit times were comparable to *Stat6*$^{-/-}$ mice infected with WNV or Hpb alone (Fig 5D). The coinfected or WNV-only infected *Stat6*$^{-/-}$ mice also showed low, if any, levels of bacteria in their spleens (Fig 5E), and similar numbers of WNV-specific CD8^{+} T cells at 10 dpi (Fig 5F). Thus, coinfection-associated gut abnormalities and defective WNV-specific immune responses require STAT6-mediated signaling events.

Bacterial translocation compromises CD8^{+} T cell responses.

To determine whether the defect in WNV-specific CD8^{+} T cells in coinfected mice was due to systemic translocation of gut bacteria, we inhibited bacterial dissemination by administering meropenem, a broad-spectrum antibiotic, twice daily via intraperitoneal route (i.p) route starting at day 5 after WNV infection (Fig 5G). Meropenem treatment did not greatly affect an established CD8^{+} T cell response in WNV-only infected mice but did rescue WNV-specific CD8^{+} T cell responses in coinfected mice (Fig 5H). The reversal in antiviral CD8^{+} T cell response correlated with reduced bacterial burden in the spleen and similar trends in the blood of meropenem-treated coinfected mice (Fig 5I-J). To corroborate these findings, we depleted gut bacteria with oral antibiotics (vancomycin, neomycin, and ampicillin [VNA]) beginning at day 5 after WNV infection, and then examined effects on WNV-specific CD8^{+} T cell responses (Fig S5D). Oral VNA treatment administered 5 days after viral infection had little impact on the numbers WNV-specific CD8^{+} T cells in WNV-only infected mice (Fig S5E). However, and similar to results with meropenem, oral VNA treatment rescued WNV-specific CD8^{+} T cell defects in coinfected mice, and this result correlated with diminished bacterial burden in blood and spleen (Fig S5E-G). Collectively, these data suggest that dissemination of gut bacteria to lymphoid tissues is largely responsible for the impaired WNV-specific CD8^{+} T cell response during coinfection.

IL-4/anti-IL-4 antibody complex treatment and WNV infection causes similar disease to Hpb and WNV coinfection.

IL-4, which activates STAT6, is a cytokine involved in polarization of type 2 responses (Finkelman et al., 2000). Because of the dependence of the coinfection phenotypes on STAT6, we tested the impact of IL-4 signaling on WNV pathogenesis in the absence of Hpb coinfection. We pre-treated WT mice with IL-4/anti-IL-4 antibody complexes (IL-4c) via an i.p. route for two days, which results in sustained release of IL-4 (Jenkins et al., 2011). The following day, IL-4c or PBS-treated control mice were inoculated with WNV, and then monitored (Fig 6A). Mice receiving IL-4c and WNV had less survival (20%) and greater weight loss than mice treated with PBS and infected with WNV or treated with IL-4c alone (Fig 6B-C). Similarly, IL-4c treatment also resulted in higher lethality rates after POWV infection (Fig S6A). At 10 dpi, we observed higher WNV burden in the brain, spinal cord and throughout the GI tract of mice given IL-4c and WNV than in the WNV-only infected group (Fig 6D). The combination of IL-4c treatment and WNV or POWV infection resulted in similar macroscopic changes as seen during coinfection, including dilated and blackened bowel (Fig 6E and S6B). The GI transit time of mice treated with IL-4c and infected with WNV was greater than mice treated with IL-4c alone and trended higher than mice infected with WNV alone (Fig 6F). Mice treated with IL-4c, infected with WNV, and then given FITC-dextran by oral gavage at 10 dpi also showed higher levels in serum than WNV-only infected mice indicating greater intestinal permeability (Fig S6C). At 10 dpi, we found markedly reduced numbers of WNV-specific $CD8^+$ T cells in infected mice receiving IL-4c (Fig 6G). Finally, we confirmed that the effects of IL-4c treatment on WNV pathogenesis required STAT6 signaling, as *Stat6*$^{-/-}$ mice treated with IL-4c did not show enhanced lethality or abnormal gut morphology (Fig 6H-I).

To determine whether viral tropism for GI tract tissues in the presence of type 2 immune skewing is necessary to cause defects in $CD8^+$ T cell response, we assessed the impact of IL-4c treatment on lymphocytic choriomeningitis virus (LCMV, Armstrong strain), which does not appreciably infect the GI tract (Beura et al., 2015). Subcutaneous inoculation of mice in the foot generated a robust LCMV-specific $CD8^+$ T cells response in the spleen, which was minimally (2-fold) reduced by IL-4c treatment (Fig S6D). Moreover, IL-4c treatment did not cause bacteremia, bacterial infection in the spleen, or macroscopic gut pathology in LCMV-infected mice (Fig S6E-G). These data suggest that type 2 immune skewing by itself has relatively minor compromising effects on antiviral $CD8^+$ T cell responses.

Expression of IL-4Rα on intestinal epithelial cells is required for Hpb-induced susceptibility to WNV.

To address how type 2 responses induced during enteric helminth infection enhance susceptibility to WNV, we performed coinfection experiments in mice with a conditional deletion of the α-subunit of the IL-4 receptor (IL-4Rα). Prior studies implicated helminth-induced M2 macrophages, activated through IL-4Rα signaling, in enhanced susceptibility to *Mtb*, MNoV, and murine gammaherpesvirus (Monin et al., 2015; Osborne et al., 2014; Reese et al., 2014). To test whether this mechanism regulates disease after Hpb and WNV coinfection, we generated LysM-Cre^+ IL-$4R\alpha^{fl/fl}$ mice, which deletes *Il4ra* in macrophages,

neutrophils, monocytes, eosinophils and some DCs (Shi et al., 2018). As a control, we also inoculated these mice with WNV or Hpb alone. We found no differences in susceptibility when LysM-Cre^{+} IL-4Rα$^{fl/fl}$ mice were singly-infected with WNV or Hpb compared to Cre^{-} IL-4Rα$^{fl/fl}$ controls. When LysM-Cre^{+} IL-4Rα$^{fl/fl}$ mice were coinfected with Hpb and WNV, 30% of them survived, similar to the Cre^{-} IL-4Rα$^{fl/fl}$ control mice (Fig 7A), with both groups showing macroscopic changes in gut morphology at 10 dpi (Fig 7B). We infected Vav-Cre^{+} IL-4Rα$^{fl/fl}$ mice, which lack IL-4Rα expression on all hematopoietic cell lineages and endothelial cells (Georgiades et al., 2002; Ogilvy et al., 1998). Again, WNV or Hpb infection alone did not result in enhanced lethality in Vav-Cre^{+} IL-4Rα$^{fl/fl}$ mice compared to the control Cre^{-} IL-4Rα$^{fl/fl}$ mice. Coinfection showed similarly enhanced lethality and macroscopic changes in the GI tract of both Vav-Cre^{+} IL-4Rα$^{fl/fl}$ and Cre^{-} IL-4Rα$^{fl/fl}$ mice (Fig 7C-D). We next infected Villin-Cre^{+} IL-4Rα$^{fl/fl}$ mice, which deletes *Il4ra* in intestinal epithelial cells. When Villin-Cre^{+} IL-4Rα$^{fl/fl}$ mice were inoculated with WNV or Hpb alone, no differences in survival were observed compared to control Cre^{-} IL-4Rα$^{fl/fl}$ mice. However, when Villin-Cre^{+} IL-4Rα$^{fl/fl}$ mice were coinfected, they failed to develop the increased lethality (Fig 7E) or macroscopic alterations of the GI tract (Fig 7F) unlike the control Cre^{-} IL-4Rα$^{fl/fl}$ mice. Thus, IL-4 signaling in intestinal epithelial cells contributes to Hpb-induced susceptibility to WNV infection and disease.

To corroborate these results, we tested whether the increased susceptibility to WNV during IL-4c treatment also required IL-4Rα expression in intestinal epithelial cells. When Cre^{-} IL-4Rα$^{fl/fl}$ control mice were treated with IL-4c and infected with WNV, 10% of them survived. In contrast, 90% of the Villin-Cre^{+} IL-4Rα$^{fl/fl}$ mice survived IL-4c treatment and WNV infection (Fig 7G) and did not sustain the macroscopic GI changes observed at 10 dpi (Fig 7H). Thus, and similar to the coinfection experiments, enhanced IL-4c-mediated susceptibility to WNV infection requires IL-4Rα expression on intestinal epithelial cells.

Exacerbated disease following WNV and Hpb coinfection requires tuft cells.

Type 2 immune responses following helminth infection result in expansion of ILC2 and Th2 immune cells and production of cytokines, including IL-4 (Allen and Maizels, 2011). Indeed, Hpb-infection resulted in increased ILC2 and Th2 cell numbers and higher IL-4 levels in the MLNs compared to uninfected or WNV-only infected mice (Fig S7A-C). However, type 2 immune responses were not changed by WNV infection, since both Hpb-infected and coinfected mice had comparable levels of ILC2 and Th2 cells and IL-4, consistent with the equivalent numbers of Hpb eggs in the stool of these mice (Fig S7A-C and Fig S1D).

Type 2 immune responses in the GI tract are initiated by tuft cells, a specialized intestinal cell lineage that detects colonization by helminths (Gerbe et al., 2016). To determine whether tuft cells contribute to the Hpb and WNV coinfection phenotypes, we utilized *Pou2f3*$^{-/-}$ mice that specifically lack tuft cells (Gerbe et al., 2016). Infection of *Pou2f3*$^{-/-}$ mice with Hpb alone did not result in mortality, and infection with WNV alone resulted in 75% survival, similar to WT mice (81%) (Fig 7I). Coinfection with Hpb and WNV in *Pou2f3*$^{-/-}$ mice, however, did not result in enhanced mortality, morphological changes in the GI tract, or impaired WNV-specific CD8^{+} T cell responses (Fig 7I-K). Furthermore, WNV

antigen staining of enteric neurons of the myenteric plexus was not enhanced in *Pou2f3*$^{-/-}$ Hpb and WNV coinfected mice, which correlated with an intact neuronal network (Fig S7D-F). Thus, tuft cells are required for the Hpb-mediated enhanced disease following WNV infection. Since IL-4/IL-13 signaling in the GI tract epithelium occurs downstream of tuft cell activation during helminth infection (Ting and von Moltke, 2019), we tested whether IL-4c treatment bypasses the need for tuft cells to cause enhanced lethality. Indeed, IL-4c treatment and WNV infection in *Pou2f3*$^{-/-}$ mice resulted in lower survival rates (18%) similar to WT mice (Fig S7G). *Pou2f3*$^{-/-}$ mice that received a combination of IL-4c and WNV also showed gut pathology at 10 dpi, whereas WNV-infection or IL-4c treatment alone of *Pou2f3*$^{-/-}$ mice did not (Fig S7H). Together, these results indicate that a tuft cell-IL-4Rα-intestinal epithelial cell signaling axis is required for Hpb-mediated exacerbated disease following WNV infection.

Tuft cells initiate type 2 responses by secreting the cytokine IL-25 (von Moltke et al., 2016). Upon Hpb infection, IL-25 levels in the SI were greater than in uninfected mice and not affected by WNV infection (Fig S7I). We determined whether the tuft cell-derived type 2 cytokine IL-25 enhances WNV susceptibility in the absence of helminth coinfection. When WT mice were treated with recombinant IL-25 and inoculated with WNV, 10% of mice survived through 11 dpi whereas 86% of the PBS-treated group survived WNV infection (Fig 7L). Mice receiving IL-25 and WNV also showed macroscopic GI changes at 10 dpi (Fig 7M). Among intestinal epithelial cells, tuft cells selectively express the succinate receptor SUCNR1, and succinate sensing can initiate the tuft cell-ILC2 circuit (Nadjsombati et al., 2018). To test whether lumenal succinate sensing alters susceptibility to WNV, we provided helminth-free WT mice with succinate in drinking water one week before WNV inoculation and throughout the time course of the experiment. All succinate-treated mice died following WNV infection by 12 dpi (Fig 7N), and this was associated with similar macroscopic GI changes observed with coinfection, IL-4c treatment, or IL-25 treatment (Fig 7O). However, succinate-treated *Pou2f3*$^{-/-}$ mice survived WNV infection and did not show the severe gut pathology, suggesting that succinate signals via tuft cells to enhance GI tract susceptibility to WNV (Fig 7N-O). Finally, succinate receptor deficient mice (*Sucnr1*$^{-/-}$) lacked macroscopic gut pathology or altered WNV-specific CD8^{+} T cell responses following WNV and Hpb coinfection (Fig S7J-K). Collectively, these results suggest that Hpb-mediated activation of type 2 responses in intestinal epithelial cells depends on tuft cells, and is possibly initiated by succinate sensing.

DISCUSSION

We established that coinfection with an enteric helminth enhances host susceptibility to WNV, a mosquito-transmitted neuroinvasive pathogen. Coinfection of mice with Hpb and WNV resulted in elevated viral burden in GI tract and CNS tissues and greater mortality. Enteric neurons of the myenteric plexus were infected with WNV to a greater extent in coinfected mice resulting in altered neuronal networks. Profound macroscopic and microscopic changes were apparent in the GI tract of coinfected mice, with barrier defects facilitating the translocation of commensal bacteria into circulation. As a consequence, the splenic architecture likely was disrupted, and WNV-specific CD8^{+} T cells responses collapsed. Coinfection in *Stat6*$^{-/-}$ mice and IL-4c treatment indicated that helminth-induced

type 2 responses were responsible for the increased mortality and associated pathology. Unexpectedly, deletion of IL-4Rα from intestinal epithelium and not from hematopoietic cells, rescued coinfected mice from increased WNV susceptibility. Thus, type 2 signaling within intestinal epithelium is critical for this pathological circuit. Finally, *Pou2f3*$^{-/-}$ or *Sucnr1*$^{-/-}$ mice that lack tuft cells or succinate receptors were protected from coinfection-induced mortality and GI tract disease, whereas treatment of helminth-free mice with the tuft cell-derived cytokine IL-25 or tuft cell ligand succinate enhanced WNV disease. These findings suggest that coinfection with enteric helminths can enhance host vulnerability to severe systemic flavivirus infections via activation of a succinate-tuft cell-IL-25-IL-4R-intestinal circuit. Type 2 immune responses may condition the enteric neurons to become more susceptible to WNV infection and injury, which could affect signals that regulate epithelial cell regeneration (Vergnolle and Cirillo, 2018), gut morphology, barrier function, and the ensuing systemic adaptive antiviral responses to neurotropic flavivirus infection (modeled in Fig S8).

Prior studies reported that enteric helminth coinfection can be beneficial to the host for respiratory viral infections and detrimental for an enteric virus infection (Furze et al., 2006; McFarlane et al., 2017; Osborne et al., 2014; Scheer et al., 2014). We showed that enteric helminth coinfection with neuroinvasive flaviviruses that have tropism for the GI tract can worsen disease severity and outcome. An emerging theme from these studies is that if the helminth and virus co-infect a common tissue, the outcome is detrimental. This may be because helminths and viruses evoke disparate immune responses. The tissue infected with a helminth must switch rapidly from a type 2 to a type 1 immune response to curtail replication of a nascent viral infection. Likely, the type 2 immune program induced by the helminth impairs local antiviral responses resulting in failure of virus containment. Moreover, induction of proinflammatory mediators in response to virus infection could worsen the wound healing response to helminth-induced damage (Allen and Sutherland, 2014; Martin and Leibovich, 2005). In support of this hypothesis, the outcome of respiratory virus coinfection was deleterious when certain helminths (*Nippostrongylus brasiliensis* or *Ascaris suum*) migrate into the lungs (Nayak and Kelley, 1965; Wescott and Todd, 1966). Similarly, coinfection with helminths that invade the liver during LCMV infection resulted in greater hepatotoxicity (Edwards et al., 2005). In contrast, enteric helminth infection was beneficial to outcome when viruses infected distant sites such as the lung (Furze et al., 2006; King et al., 2017). In such situations, enteric helminths and the ensuing immune responses can alter leukocyte trafficking or activation and limit pathological inflammation. These observations suggest that the tissue niche of co-infection can determine outcome.

One consequence of the loss of barrier integrity was a collapse of WNV-specific CD8$^+$ T cells in the spleen of coinfected mice. T cell priming appeared normal, as WNV-specific CD8$^+$ T cell responses were equivalent in number and activation in WNV-only and coinfected mice at day 7. However, by day 8, increased annexin V expression was observed preferentially on WNV-specific CD8$^+$ T cells of coinfected mice, suggesting the loss of a pro-survival signal or gain of a pro-death signal after priming. This survival signal could be DC-derived, since we noted that DCs were absent in T cell zones of the spleen in coinfected mice. Since antibiotic treatment of coinfected mice rescued the CD8$^+$ T cell defects, it appears that bacterial translocation from the GI tract and systemic spread to lymphoid

tissues contributes to the decline of antiviral $CD8^+$ T cells. In contrast, IL-4 treatment during infection with LCMV did not cause bacterial translocation and induced only minor defects in antiviral $CD8^+$ T cell response. Consistent with our results, translocation of gut bacteria in some sepsis models preferentially affects $CD8^+$ T cells, DCs, and NK cells (Danahy et al., 2016; Jensen et al., 2018), and intravenous administration of *E. coli* dampened LCMV-specific $CD8^+$ T cell responses (Straub et al., 2018).

Our findings contrast with a study that examined coinfection with another enteric helminth, *Trichinella spiralis* (Ts), and an enteric MNoV infection (Osborne et al., 2014). Unlike the MNoV model, in which elevated viral burden was observed only in the distal SI of coinfected mice, we observed higher WNV burden in multiple GI tract segments as well as CNS tissues, which impacted clinical outcome. We did not detect proliferation defects in virus-specific $CD8^+$ T cells as reported in the Ts/MNoV coinfection study but instead observed increased cell death. In both studies, STAT6 responses mechanistically played a role but the specific aspects of type 2 immunity were distinct. In the Ts/MNoV coinfection study, impaired $CD8^+$ T cell responses were attributed to IL-4 skewing of macrophages to an alternatively activated state, as has been reported in other studies (Monin et al., 2015; Reese et al., 2014). However, during Hpb and WNV coinfection, a lack of IL-4Rα expression on myeloid (LysM-Cre^+ IL-4$R\alpha^{fl/fl}$) or other hematopoietic cells (Vav-Cre^+ IL-4$R\alpha^{fl/fl}$) did not affect GI tract pathology or mortality. In contrast, a lack of IL-4Rα signaling in intestinal epithelium (Villin-Cre^+ IL-4$R\alpha^{fl/fl}$) rescued the coinfected mice from severe disease. These data suggest that the IL-4 and STAT6 response acts intrinsically in intestinal epithelium after Hpb and WNV co-infection to contribute to disease pathogenesis.

Tuft cells are chemosensing intestinal epithelial cells whose role during viral infection remains poorly defined because of their relatively low frequency (Ting and von Moltke, 2019). Nonetheless, tuft cells expand after detecting enteric helminths and protists (Ting and von Moltke, 2019). We found that *Pou2f3*$^{-/-}$ mice lacking tuft cells were resistant to coinfection-induced lethality. Tuft cell-derived signals induce GI tract remodeling in the intestinal epithelium and lamina propria, which could impact tropism, as seen for MNoV (Wilen et al., 2018). Alternatively, tuft cell-derived signals could modulate the downstream consequences of WNV infection in neurons of the myenteric plexus (White et al., 2018) including alterations of neuronal networks. Although the precise signals that affect the permissiveness of enteric neurons remains unknown, cross-talk between type 2 immunity and enteric nervous system neurons was recently described (Moriyama and Artis, 2019). Moreover, inputs from enteric neurons are important for epithelial cell regeneration and maintaining barrier integrity, and neuronal damage by WNV could disrupt this communication signal (Vergnolle and Cirillo, 2018). Coinfection caused greater turnover and shedding of intestinal epithelial cells resulting in villus blunting and focal tufting along the lining of the proximal SI. Our finding that IL-25 treatment in the absence of helminths exacerbated WNV infection-induced gut pathology is consistent with tuft cells providing a key initiating pathological signal. Recently, succinate was discovered as a tuft cell activation ligand, and the succinate receptor SUNCR1 was found exclusively on tuft cells among intestinal epithelial cell lineages (Nadjsombati et al., 2018). Indeed, when we treated helminth-free mice with succinate and then infected them with WNV, we observed GI pathology and mortality, suggesting that lumenal succinate sensing by tuft cells adversely

affected WNV disease outcome. While we do not know if succinate is the trigger for enhanced WNV disease during coinfection, *Sucnr1*$^{-/-}$ mice lacked gut pathology or altered WNV-specific CD8^{+} T cell responses following WNV and Hpb coinfection. Consistent with this observation, succinate-producing commensal bacteria are enriched during helminth infection in the context of changes to the microbiome (Lei et al., 2018). Alternatively, succinate could be derived from helminths themselves (Nadjsombati et al., 2018).

The geographical overlap between WNV and enteric helminth infections principally is restricted to the African subcontinent and parts of Eastern Europe (Hotez et al., 2008; Sule et al., 2018). However, several other mosquito-transmitted flaviviruses are endemic in areas of the world with high helminth burden including South America, the Indian subcontinent, and Southeast Asia (Daep et al., 2014). Although we used WNV as a model for dissecting the mechanisms for enhanced host susceptibility, similar findings were observed with other neurotropic flaviviruses that can infect the myenteric plexus of the GI tract (White et al., 2018). Future studies will be required to define the impact of enteric helminth infection on host immunity to neurotropic and viscerotropic flaviviruses in humans and other susceptible vertebrate animals.

During helminth or protist infections alone, overt injury to the host GI tract is not observed upon activation of tuft cells, except for lengthening of the small intestine to accommodate metabolic needs (Schneider et al., 2018). Only when mice were co-infected with helminths and WNV, did we observe functional damage to the GI tract. Thus, helminth-mediated GI remodeling, which likely protects against worm re-challenge, can adversely affect a heterologous virus challenge. Future studies that elucidate the mechanistic relationships between neuronal inputs, tuft cells, type 2 immunity, and barrier integrity in the context of coinfection may reveal paradigms as to how the neuroimmune axis in the GI tract contributes to protection or damage against pathogen-induced tissue injury. Moreover, epidemiological studies are needed to define the impact of other helminth infections (*e.g.*, flukes, tapeworms, and roundworms) on the outcome of systemic and enteric viral infections that target different cells and regions of the GI tract.

STAR METHODS

RESOURCE AVAILABLITY

Lead Contact.—Further information and requests for resources and reagents should be directed to and will be fulfilled by the Lead Contact, Michael S. Diamond (diamond@wusm.wustl.edu).

Materials Availability.—All requests for resources and reagents should be directed to and will be fulfilled by the Lead Contact author. This includes mice, antibodies, viruses, and helminths. All reagents will be made available on request after completion of a Materials Transfer Agreement.

Data and code availability.—All data supporting the findings of this study are available within the paper and are available from the corresponding author upon request.

EXPERIMENTAL MODEL AND SUBJECT DETAILS

Mouse experiments.—This study was conducted in strict accordance with the recommendations of the Guide for the Care and Use of Laboratory Animals of the National Institutes of Health. Animal experiments were performed as specified in protocols approved by the Institutional Animal Care and Use Committee (IACUC) at the Washington University School of Medicine (Assurance Number: A3381-01). All dissections and inoculations were performed under anesthesia, induced and maintained by using ketamine hydrochloride and xylazine and every effort was made to minimize suffering.

C57BL/6J WT mice (000664) were purchased directly from Jackson Laboratories. *Stat6*^{tm1Gru} (*Stat6*$^{-/-}$) (005977) were purchased from Jackson Laboratories and bred at Washington University under specific pathogen-free conditions. *Il4ra*$^{fl/fl}$ mice on a C57BL/6J background were obtained from Dr. Ajay Chawla (University of California, San Francisco) and crossed with different Cre recombinase mice (Vav$^{+/-}$ Cre; B6.Cg-Commd10$^{Tg(Vav1-icre)A2Kio}$/J, Villin$^{+/-}$ ^{B6}·Cre; B6.Cg-Tg(Vil1-cre)997Gum/J, LysM$^{+/-}$ Cre; B6.129P2-Lyz2$^{tm1(Creasy\ et\ al.)Ifo}$/J) to generate cell-specific deletions of the IL-4Rα subunit. Cre recombinase mice were obtained from Jackson Laboratories: (Vav-Cre (008610), Villin-Cre (004586), LysM-Cre (004781)) and bred at Washington University. *Pou2f3*$^{-/-}$ mice were developed with assistance from the Genome Engineering and iPSC 556 Center (GEiC) at Washington University in Saint Louis. Small guide sgRNA 5'-AGGCCATGCCACCTGAGCCANGG-3' was designed to target the *Pou2f3* locus in the fourth exon. C57BL/6J (Jackson Laboratories, Bar Harbor, ME) fertilized zygotes were injected with Cas9 mRNA and sgRNA. A founder mouse with the following mutation was recovered: WT CCCACAGGCCATGCCACCTGAGCCAAGGAC; KO CCCACAGGCCT---------CTCCCAAGGAC. *Sucnr1*$^{-/-}$ mice were kindly provided by Jakob von Moltke (University of Washington). Age-matched (9 or 10-week old) male mice and their littermate controls were used in all WNV and POWV experiments. ZIKV infection experiments were performed in 4-week old WT male mice. All transgenic mice were genotyped by real-time PCR (Transnetyx). All mice were fed a 2% protein diet (PicoLab 5053, Purina) and maintained on a 12 h light/dark cycle.

Viruses.—WNV strain 3000259, New York 2000 was propagated in C6/36 *Aedes albopictus* cells as described (Brien et al., 2013). Mouse-adapted ZIKV (strain Dakar 41525) was propagated as described (Gorman et al., 2018). POWV (strain FB5/13-#1) was produced as described (VanBlargan et al., 2018). Virus stocks were tittered on Vero cells by focus-forming assay (Brien et al., 2013). Stocks of LCMV (Armstrong strain) were propagated in BHK21 cells and tittered on Vero cells by focus-forming assays.

Helminths.—Hpb third-stage larvae (L3) were generated as described (Camberis et al., 2003). Hpb L3 viability was checked by microscope for motility, and their numbers were quantified before use. Mice were gavaged with 200 Hpb L3 or PBS (control) using 20-gauge x 38 mm plastic feeding tubes (Instech; FTP-20-38). Twelve days after inoculation with Hpb L3, mice were inoculated subcutaneously in the footpad with 10^2 FFU of WNV, 10^2 FFU of POWV, 10^6 FFU of ZIKV or 10^3 FFU of LCMV in 50 μl of PBS. Mice treated with IL-4c, IL-25 and succinate also were infected with the same doses of WNV and POWV. In some

experiments, mice were gavaged with 2.5 mg/ml of the anti-helminthic drug pyrantel pamoate (Columbia Laboratories) on two consecutive days (day −2, day −1) prior to WNV infection (day 0).

METHOD DETAILS

Helminth egg enumeration.—Fresh fecal pellets were collected at indicated time points and eggs per gram of feces were enumerated as a readout of worm fitness (Li et al., 2018). Briefly, two to three fecal pellets were collected from each mouse, weighed and homogenized in 2 ml of distilled H_2O with 2% paraformaldehyde (PFA). Two ml of saturated NaCl solution was added to each tube, mixed and allowed to settle for 5 to 10 min for the eggs to float on the top. Using a sterile pipette, 400 μl of the mixed solution was loaded onto McMaster 2-chamber egg counter. The worm eggs were counted within the grid and the eggs per gram feces were determined by the following formula: eggs/g = egg counts x 26.67 weight of feces (g). The 26.67 in the formula is obtained from the total volume in which the fecal pellets are suspended (4 ml) divided by the volume within the grid (0.15 ml).

Viral RNA extraction and quantification.—At specific days after virus inoculation, anesthetized mice were perfused with 20 ml of sterile PBS. Subsequently, tissues were harvested in sterile 2 ml tubes and stored at −80°C. Frozen tissues were thawed, weighed and homogenized in 0.3 to 0.5 ml of DMEM supplemented with 2% FBS containing ceramic beads using a MagNA Lyser tissue homogenizer (Roche). RNA was extracted from 50 μl of homogenate using an Applied Biosystems 5x MagMax RNA viral isolation kit (Thermo Scientific) and a Kingfisher duo prime extraction machine (Thermo Scientific). All viral RNA quantifications were performed using one-step qRT-PCR on a 7500 Fast Real Time-PCR system (Applied Biosystems). WNV genome copies were quantified using WNV-specific primers and probes and compared to a standard curve of purified viral genomic RNA (Brien et al., 2013). Genome copies were normalized by tissue weight and expressed as $\log_{10}$ genome copies of RNA or FFU equivalents per gram of tissue using a standard curve.

GI tract motility measurements.—GI tract motility was measured using a carmine red dye assay (White et al., 2018). Briefly, 6% (w/v) carmine red dye (Sigma Aldrich) was dissolved in sterile distilled water containing 0.5% methyl cellulose (Sigma Aldrich). Mice were gavaged with 300 μl of carmine dye solution, and 3 h later placed individually in empty cages to check for emergence of red fecal pellets over 6 h.

Immunohistochemistry and whole mount staining.—Intestinal sections were harvested at indicated times after inoculation, opened along the mesenteric border, pinned to Sylgard silicon plates, and fixed in 10% neutral buffered formalin overnight at 4°C. Following dehydration in sequential ethanol (30%, 50% and 70%) washes, the tissues were blocked in 2% agar and stored in 70% ethanol at 4°C. Subsequently, paraffin embedding, sectioning, and staining with hematoxylin and eosin was performed (Developmental Biology Core Facility, Washington University School of Medicine).

For WNV antigen staining in intestinal sections, tissues were deparaffinized by three sequential incubations in xylene followed by three sequential washes in isopropanol. Antigen retrieval was performed by boiling sections in Dako Target Retrieval Solution (Dako) or Trilogy antigen retrieval solution (Cell Marque) for 20 min followed by a 10-min incubation at room temperature. Slides were blocked for 30 min at room temperature in Tris-HCl (25 mM, pH 7.4) or PBS buffered solutions containing 1% bovine serum albumin (BSA), 5% normal donkey serum, and 0.05% Tween-20. Sections were incubated overnight at 4°C with rat anti-WNV hyperimmune serum (1:400, (Diamond et al., 2003)), rabbit anti-Tuj1 polyclonal serum (1:500, Sigma Aldrich, catalog # T2200). Primary antibodies were detected with Cy3-conjugated donkey anti-rat (Jackson Laboratories) or Alexa Fluor 488-conjugated donkey anti-rabbit antibodies (ThermoFisher) diluted in blocking buffer for 60 min at room temperature. Following counter staining with Hoechst 33342 dye (Thermo Fisher), tissue sections were mounted in ProLong Gold anti-fade (Thermo Fisher) and stored at 4°C until imaging. For the cell death assay, antigen retrieval and permeabilization was performed as described above prior to TUNEL staining using *In Situ* Cell Death Detection kit (Roche, # 12156792910) according to the manufacturer's instructions.

For whole mount staining, pinned tissues were fixed in 10% neutral buffered formalin overnight at 4°C. Following three washes in PBS, the muscularis propria was dissected from the mucosa under a dissecting microscope and stored at 4°C in PBS and 0.02% NaN_3. Tissues were blocked for 1 h at room temperature (Blocking buffer: TBS (WNV antigen staining) or PBS (nNOS and calretinin staining) + 5% donkey serum + 1% BSA + 1% Triton X-100) and incubated overnight with primary antibodies (nNOS (Abcam; Ab1376), calretinin clone DC8 (Thermofisher, 180211), Iba1 (Abcam; Ab178846), anti-WNV polyclonal serum (Diamond et al., 2003)) at 4°C. Following three washes in PBS + 1% Triton X-100, the tissues were incubated for 1 h at room temperature with the following secondary antibodies: donkey anti-rabbit Alexa Fluor 488 or 647 (Thermofisher, A31573 and A21206), donkey anti-goat Alexa Fluor 488 (Thermofisher, A11055) and donkey anti-rat Alexa Fluor 594 (Thermofisher, 21209) in PBS or TBS + 3% donkey serum + 1% BSA +1% Triton X-100. Subsequently, tissue sections were washed three times in PBS + 1% Triton X-100, counterstained for nuclei with Hoechst 33342 dye (Thermo Fisher) and mounted in Aqua-Poly/Mount (Polysciences). Sections were imaged with Zeiss LSM880 Laser Scanning Confocal microscope using 20x (NA 0.8) or 40x (NA 1.4) objectives. The scanned images were processed and analyzed by Fiji software (http://fiji.sc/Fiji). For quantification of neuronal density, five random regions (0.65 mm^2) of 20x magnification area were scanned and stitched (ZEN black software, Zeiss). To determine the level of WNV infection, regions of tissue of 4 mm^2 size were scanned and stitched (ZEN black software, Zeiss). For all images, the background signal was uniformly subtracted (rolling ball, radius 50). Quantification was performed by converting images to binary using a threshold tool, and a fraction of total area was measured. For calretinin and nNOS positive areas, the median value from each 5 images was calculated for every mouse and normalized to values in naïve mice. The amount of WNV infection (% of total area with WNV-antigen staining) in coinfected mice was expressed as the fold change of values of sections obtained from WNV-only infected mice. Sections from naïve mice served as negative controls.

Gut bacterial leakage assays.—Gut bacterial leakage was determined as described (Liu et al., 2019). In brief, spleens of naïve or infected mice were harvested at specified time points in a 15-ml conical containing 2 ml of sterile DMEM without antibiotics or FBS. Spleens were minced into small pieces with a sterile scissors to avoid contamination. Sterile DMEM (3 ml, no antibiotics or FBS) was added to samples, and two sequential dilutions (1:10 and 1:100) were made by taking 1 ml from the 5-ml sample using same sterile DMEM. Samples were plated on blood agar plates (Fisher Scientific; 221239) using an L-shaped spreader. Plates were incubated with at 37°C overnight and on the next day, the number of colonies were counted. Approximately 300 to 400 μl of blood was aspirated from the thoracic cavity of each mouse using sterile 1 ml syringe and transferred to blood collection tube containing EDTA (Becton Dickinson; 365971). After two sequential dilution in sterile DMEM (no antibiotics, no FBS), 100 μl of blood was plated on blood agar plates, incubated overnight at 37°C and colonies were quantified on the next day.

A FITC-dextran assay was used to measure intestinal permeability (Stanley et al., 2016). Mice were gavaged with 150 μl of FITC-dextran (3-5 kDa; Sigma) at 80 mg/ml in sterile PBS. Mice were euthanized 4-h later, and blood was collected into serum separator tubes. Tubes were centrifuged at 10,000 x rpm for 10 min, serum was transferred to new sterile tubes and diluted 1:1 with 2% Triton X-100. Serum fluorescence intensities were measured at 485 nm excitation/528 nm emission using a Synergy H1 Hybrid Multi-mode Microplate Reader (BioTek Inc.).

Flow cytometry analysis.—Tissues (spleen, brain and lymph nodes) were harvested at specified times after virus inoculation. All mice were anesthetized and perfused with 20 ml of sterile PBS, and tissues were collected in 2-ml tubes containing 1 ml of fresh DMEM. Spleen and lymph nodes were dispersed into single cell suspension using a 70 μm cell strainer. Erythrocytes were lysed using ACK lysis buffer, and cells were resuspended in DMEM with 10% FBS. An aliquot was taken for cell counting and ~2-4 x 10^6 cells were plated in 96-well round-bottom plates and incubated with antibodies against different antigens. Brain samples were minced in small pieces and incubated for 45 min with digestion buffer containing 0.05% collagenase D, 10 μg/ml of DNase in HBSS supplemented with 10 mM HEPES (pH 7.4; Life Technologies). The brain digest was pushed through a 70 μm cell strainer, washed and resuspended in 10 ml of 30% Percoll solution and centrifuged for 30 min (1,200 x rpm at 4°C, no brake). The top myelin layer was removed using a transfer pipette, and the supernatant was discarded. The pellet was resuspended in 1 ml of FACS buffer (2% FBS, 2 mM EDTA, 0.1% NaN_3) and stained with antibodies.

For staining of surface antigens (spleen, brain and MLN), cell suspensions were stained with fluorophore conjugated antibody cocktail containing Viability Dye (eBiosciences; 506), Fc block (BD Biosciences; clone 2.4G2), CD45 (BD Biosciences; clone 30-F11), B220 (BioLegend; clone RA36B4), CD3 (BD Biosciences; clone 145-2c11), CD8a (BioLegend; clone 53-6.7), CD4 (BioLegend; clone RM4-5), CD44 (BioLegend; clone IM7), KLRG1 (eBiosciences; clone 2F1), CD127 (eBiosciences; clone A7R34) and WNV specific D^b-immunodominant NS4B tetramer (NIH Tetramer Core Facility; SSVWNATTA) in FACS buffer for 45 min at 4°C. Subsequently, cells were washed with FACS buffer, fixed using 4%

PFA for 5 min at room temperature, and washed again with FACS buffer. Cells were resuspended in 200 μl of FACS buffer and analyzed on a BD X-20 flow cytometry machine within 3 days. For staining of intracellular antigens in T cells, cells were washed with FACS buffer, fixed and permeabilized using Foxp3 staining kit according to the manufacturer's protocol (eBiosciences; 00552300), and then stained with anti-T-bet (Invitrogen; clone 4B10), anti-Ki67 (eBiosciences; clone SolA15), anti-Foxp3 (BD Biosciences; clone MF23) or anti-GATA3 (BD Biosciences; clone L50-823) antibodies for 45 min at room temperature. For Annexin V staining, cells were stained according to the manufacturer's protocol (BioLegend; 640905), kept in Annexin V binding buffer with 2% PFA, and processed on a BD x-20 Flow cytometer on the same day. For myeloid cell staining, cells were stained with Viability Dye (eBiosciences; 506), Fc block (BD Biosciences; clone 2.4G2), CD45 (BD Biosciences; clone 30-F11), CD3 (BD Biosciences; clone 145-2c11) [negative cells], B220 (BioLegend; clone RA36B4) [negative cells], CD11b (BD Biosciences; clone M1/70), NK1.1 (BioLegend; clone PK136), Ly6G (BioLegend; clone 1A8), Ly6C (eBiosciences; clone HK1.4), Siglec F (BD Biosciences; clone E50-2440), CD11c (BD Biosciences; clone HL3), MHC-II (BioLegend; clone M1308A10) and F4/80 (eBiosciences; clone BM8). Data were analyzed using FlowJo software (Treestar, Inc.).

Immunofluorescence microscopy.—Spleens were fixed in 2 ml of periodate-lysine-paraformaldehyde (PLP) fixative (PBS containing 0.1 M L-lysine, 2% PFA, and 2.1 mg/ml $NaIO_4$ at pH 7.4) for 24 hours at 4°C and cryoprotected in 15% sucrose/PBS solution. Spleens then were embedded in OCT medium (Electron Microscopy Sciences) and frozen in dry-ice cooled isopentane. Sixteen-micron sections were cut on a Leica cryostat (Leica Microsystems), blocked with 5% goat or donkey serum then stained with antibodies against one or more of the following proteins or structures: CD11c (clone N418, eBioscience), CD8α (clone 53-6.7, eBioscience), B220 (clone RA3–6B2, eBioscience), CD169 (3D6.112, Biolegend), GL7 (clone GL7, Biolegend), CD21/35 (clone eBio4E3, eBioscience), MAdCAM-1 (clone MECA-367, eBioscience), ERTR7 (which recognizes an fibroblastic reticular cells antigen was used to identify the LN stromal network including conduits, blood vessels, and lymphatic sinuses; rat monoclonal, Abcam, 51824). Sections were incubated with secondary antibodies only as controls, and images were acquired using a Leica SP8 confocal microscope, identical PMT (photomultiplier tube) and laser settings. Images were analyzed by using Imaris software (Bitplane).

IL-4-anti-IL-4 complexes and IL-25 treatment.—IL-4c were generated as described (Jenkins et al., 2011). For each mouse, 5 μg of murine IL-4 (Peprotech) was mixed with 25 μg anti-IL-4 (BioXCell, Clone 11B11) and incubated for 15 min on ice before diluting in 200 μl total volume of PBS. IL-4c was administered via an intraperitoneal route (200 μl/mouse) on two consecutive days (day −2 and −1) relative to virus infection (day 0). In some experiments, mice were administered 500 ng/mouse of recombinant IL-25 (R&D 1399-IL-025/CF) in 100 μl of PBS via intraperitoneal route on two consecutive days (days −2 and −1) relative to virus infection.

Succinate treatment.—Mice were provided with sodium succinate hexahydrate (Alfa Aesar) *ad libitum* in drinking water at a concentration 150 mM starting 7 days prior to WNV

inoculation and continued throughout the experiment as described (Nadjsombati et al., 2018).

Antibiotic treatments.—Mice were administered 500 μg of meropenem (Sigma; PHR1772) twice daily (12 hours apart) via intraperitoneal route starting from day 5 post-WNV infection until day 9. In separate experiments, mice were administered an oral antibiotic cocktail of vancomycin, neomycin, and ampicillin (0.5 grams each per liter) in water starting from day 5 post-WNV infection until day 9 (Thackray et al., 2018).

IL-4 and IL-25 ELISA.—IL-4 and IL-25 cytokine levels were quantified from MLN or small intestinal homogenates by ELISA as per manufacturer's instructions (R & D Systems, M4000B; Thermofisher Scientific, BMS6046).

QUANTIFICATION AND STATISTICAL ANALYSIS

Statistical tests used to analyze experiments are described in the Figure Legends. Survival curves were analyzed by Bonferroni correction, weight loss was measure by one-way ordinary ANOVA with Holm-Sidak test. Viral burden, WNV antigen in muscularis and area positive for nNOS and calretinin was analyzed using the Mann-Whitney test. TUNEL staining data was analyzed by one-way ANOVA with Holm-Sidak test. Carmine red dye assay, gut bacterial burden, and FITC-dextran assay were analyzed by Kruskal-Wallis ANOVA with Dunn's post-test. Analysis of immune cell populations was performed using an unpaired t test. All data were analyzed using Prism software (GraphPad10, San Diego, CA). No statistical methods were used to predetermine sample size prior to experiments. The experiments were not randomized, and the investigators were not blinded for clinical outcome assessment. Quantitation of immunofluorescence microscopy was performed by a blinded investigator.

Supplementary Material

Refer to Web version on PubMed Central for supplementary material.

ACKNOWLEDGEMENTS

This work was supported by NIH grants R01 AI101400, R01 HD091218, R01AI145296, and R01 DK122790, and ARS-CRIS 8042-31000-107-00D. H.D.H is supported by the NIAID Division of Intramural Research. We would like to thank Jakob von Moltke for providing the *Sucnr1*$^{-/-}$ mice and Craig Wilen for development of the *Pou2f3*$^{-/-}$ mice. The model in Fig S8 was created with BioRender.com.

REFERENCES

Aguilar-Valenzuela R, Netland J, Seo YJ, Bevan MJ, Grakoui A, and Suthar MS (2018). Dynamics of Tissue-Specific CD8(+) T Cell Responses during West Nile Virus Infection. J Virol 92.

Allen JE, and Maizels RM (2011). Diversity and dialogue in immunity to helminths. Nat Rev Immunol 11, 375–388. [PubMed: 21610741]

Allen JE, and Sutherland TE (2014). Host protective roles of type 2 immunity: parasite killing and tissue repair, flip sides of the same coin. Semin Immunol 26, 329–340. [PubMed: 25028340]

Beura LK, Anderson KG, Schenkel JM, Locquiao JJ, Fraser KA, Vezys V, Pepper M, and Masopust D (2015). Lymphocytic choriomeningitis virus persistence promotes effector-like memory

differentiation and enhances mucosal T cell distribution. J Leukoc Biol 97, 217–225. [PubMed: 25395301]

Bigham AW, Buckingham KJ, Husain S, Emond MJ, Bofferding KM, Gildersleeve H, Rutherford A, Astakhova NM, Perelygin AA, Busch MP, et al. (2011). Host genetic risk factors for West Nile virus infection and disease progression. PloS one 6, e24745. [PubMed: 21935451]

Borges da Silva H, Fonseca R, Pereira RM, Cassado Ados A, Alvarez JM, and D'Imperio Lima MR (2015). Splenic Macrophage Subsets and Their Function during Blood-Borne Infections. Front Immunol 6, 480. [PubMed: 26441984]

Bouchery T, Volpe B, Shah K, Lebon L, Filbey K, LeGros G, and Harris N (2017). The Study of Host Immune Responses Elicited by the Model Murine Hookworms Nippostrongylus brasiliensis and Heligmosomoides polygyrus. Curr Protoc Mouse Biol 7, 236–286. [PubMed: 29261231]

Brien JD, Lazear HM, and Diamond MS (2013). Propagation, quantification, detection, and storage of West Nile virus. Curr Protoc Microbiol 31, 15D 13 11–15D 13 18.

Camberis M, Le Gros G, and Urban J Jr. (2003). Animal model of Nippostrongylus brasiliensis and Heligmosomoides polygyrus. Curr Protoc Immunol *Chapter 19*, Unit 19 12.

Cheng LE, and Locksley RM (2014). Allergic inflammation--innately homeostatic. Cold Spring Harb Perspect Biol 7, a016352. [PubMed: 25414367]

Creasy JM, Goldman DA, Dudeja V, Lowery MA, Cercek A, Balachandran VP, Allen PJ, DeMatteo RP, Kingham TP, D'Angelica MI, et al. (2017). Systemic Chemotherapy Combined with Resection for Locally Advanced Gallbladder Carcinoma: Surgical and Survival Outcomes. J Am Coll Surg 224, 906–916. [PubMed: 28216422]

Daep CA, Munoz-Jordan JL, and Eugenin EA (2014). Flaviviruses, an expanding threat in public health: focus on dengue, West Nile, and Japanese encephalitis virus. J Neurovirol 20, 539–560. [PubMed: 25287260]

Danahy DB, Strother RK, Badovinac VP, and Griffith TS (2016). Clinical and Experimental Sepsis Impairs CD8 T-Cell-Mediated Immunity. Crit Rev Immunol 36, 57–74. [PubMed: 27480902]

Diamond MS, Shrestha B, Marri A, Mahan D, and Engle M (2003). B cells and antibody play critical roles in the immediate defense of disseminated infection by West Nile encephalitis virus. J Virol 77, 2578–2586. [PubMed: 12551996]

Edwards MJ, Buchatska O, Ashton M, Montoya M, Bickle QD, and Borrow P (2005). Reciprocal immunomodulation in a schistosome and hepatotropic virus coinfection model. J Immunol 175, 6275–6285. [PubMed: 16272278]

Finkelman FD, Morris SC, Orekhova T, Mori M, Donaldson D, Reiner SL, Reilly NL, Schopf L, and Urban JF Jr. (2000). Stat6 regulation of in vivo IL-4 responses. J Immunol 164, 2303–2310. [PubMed: 10679064]

Furze RC, Hussell T, and Selkirk ME (2006). Amelioration of influenza-induced pathology in mice by coinfection with Trichinella spiralis. Infect Immun 74, 1924–1932. [PubMed: 16495568]

Georgiades P, Ogilvy S, Duval H, Licence DR, Charnock-Jones DS, Smith SK, and Print CG (2002). VavCre transgenic mice: a tool for mutagenesis in hematopoietic and endothelial lineages. Genesis 34, 251–256. [PubMed: 12434335]

Gerbe F, Sidot E, Smyth DJ, Ohmoto M, Matsumoto I, Dardalhon V, Cesses P, Garnier L, Pouzolles M, Brulin B, et al. (2016). Intestinal epithelial tuft cells initiate type 2 mucosal immunity to helminth parasites. Nature 529, 226–230. [PubMed: 26762460]

Gorman MJ, Caine EA, Zaitsev K, Begley MC, Weger-Lucarelli J, Uccellini MB, Tripathi S, Morrison J, Yount BL, Dinnon KH 3rd, et al. (2018). An Immunocompetent Mouse Model of Zika Virus Infection. Cell Host Microbe 23, 672–685 e676. [PubMed: 29746837]

Hildner K, Edelson BT, Purtha WE, Diamond M, Matsushita H, Kohyama M, Calderon B, Schraml BU, Unanue ER, Diamond MS, et al. (2008). Batf3 deficiency reveals a critical role for CD8alpha + dendritic cells in cytotoxic T cell immunity. Science 322, 1097–1100. [PubMed: 19008445]

Hotez PJ, Brindley PJ, Bethony JM, King CH, Pearce EJ, and Jacobson J (2008). Helminth infections: the great neglected tropical diseases. J Clin Invest 118, 1311–1321. [PubMed: 18382743]

Howitt MR, Lavoie S, Michaud M, Blum AM, Tran SV, Weinstock JV, Gallini CA, Redding K, Margolskee RF, Osborne LC, et al. (2016). Tuft cells, taste-chemosensory cells, orchestrate parasite type 2 immunity in the gut. Science 351, 1329–1333. [PubMed: 26847546]

Jenkins SJ, Ruckerl D, Cook PC, Jones LH, Finkelman FD, van Rooijen N, MacDonald AS, and Allen JE (2011). Local macrophage proliferation, rather than recruitment from the blood, is a signature of TH2 inflammation. Science 332, 1284–1288. [PubMed: 21566158]

Jensen IJ, Winborn CS, Fosdick MG, Shao P, Tremblay MM, Shan Q, Tripathy SK, Snyder CM, Xue HH, Griffith TS, et al. (2018). Polymicrobial sepsis influences NK-cell-mediated immunity by diminishing NK-cell-intrinsic receptor-mediated effector responses to viral ligands or infections. PLoS Pathog 14, e1007405. [PubMed: 30379932]

Johnston CJ, Robertson E, Harcus Y, Grainger JR, Coakley G, Smyth DJ, McSorley HJ, and Maizels R (2015). Cultivation of Heligmosomoides polygyrus: an immunomodulatory nematode parasite and its secreted products. J Vis Exp, e52412. [PubMed: 25867600]

Kau AL, Planer JD, Liu J, Rao S, Yatsunenko T, Trehan I, Manary MJ, Liu TC, Stappenbeck TS, Maleta KM, et al. (2015). Functional characterization of IgA-targeted bacterial taxa from undernourished Malawian children that produce diet-dependent enteropathy. Sci Transl Med 7, 276ra224.

King IL, Mohrs K, Meli AP, Downey J, Lanthier P, Tzelepis F, Fritz JH, Tumanov AV, Divangahi M, Leadbetter EA, et al. (2017). Intestinal helminth infection impacts the systemic distribution and function of the naive lymphocyte pool. Mucosal Immunol 10, 1160–1168. [PubMed: 28120841]

Lazear HM, Govero J, Smith AM, Platt DJ, Fernandez E, Miner JJ, and Diamond MS (2016). A Mouse Model of Zika Virus Pathogenesis. Cell Host Microbe 19, 720–730. [PubMed: 27066744]

Lee G, White LS, Hurov KE, Stappenbeck TS, and Piwnica-Worms H (2009). Response of small intestinal epithelial cells to acute disruption of cell division through CDC25 deletion. Proc Natl Acad Sci U S A 106, 4701–4706. [PubMed: 19273838]

Lei W, Ren W, Ohmoto M, Urban JF Jr., Matsumoto I, Margolskee RF, and Jiang P (2018). Activation of intestinal tuft cell-expressed Sucnr1 triggers type 2 immunity in the mouse small intestine. Proc Natl Acad Sci U S A 115, 5552–5557. [PubMed: 29735652]

Li S, Bostick JW, Ye J, Qiu J, Zhang B, Urban JF Jr., Avram D, and Zhou L (2018). Aryl Hydrocarbon Receptor Signaling Cell Intrinsically Inhibits Intestinal Group 2 Innate Lymphoid Cell Function. Immunity 49, 915–928 e915. [PubMed: 30446384]

Lindsey NP, Staples JE, Lehman JA, and Fischer M (2012). Medical risk factors for severe West Nile Virus disease, United States, 2008-2010. Am J Trop Med Hyg 87, 179–184. [PubMed: 22764311]

Liu Q, Johnson EM, Lam RK, Wang Q, Bo Ye H, Wilson EN, Minhas PS, Liu L, Swarovski MS, Tran S, et al. (2019). Peripheral TREM1 responses to brain and intestinal immunogens amplify stroke severity. Nat Immunol 20, 1023–1034. [PubMed: 31263278]

Loke P, and Lim YA (2015). Helminths and the microbiota: parts of the hygiene hypothesis. Parasite Immunol 37, 314–323. [PubMed: 25869420]

Martin P, and Leibovich SJ (2005). Inflammatory cells during wound repair: the good, the bad and the ugly. Trends Cell Biol 15, 599–607. [PubMed: 16202600]

Matheis F, Muller PA, Graves CL, Gabanyi I, Kerner ZJ, Costa-Borges D, Ahrends T, Rosenstiel P, and Mucida D (2020). Adrenergic Signaling in Muscularis Macrophages Limits Infection-Induced Neuronal Loss. Cell 180, 64–78 e16. [PubMed: 31923400]

McFarlane AJ, McSorley HJ, Davidson DJ, Fitch PM, Errington C, Mackenzie KJ, Gollwitzer ES, Johnston CJC, MacDonald AS, Edwards MR, et al. (2017). Enteric helminth-induced type I interferon signaling protects against pulmonary virus infection through interaction with the microbiota. J Allergy Clin Immunol 140, 1068–1078 e1066. [PubMed: 28196762]

Monin L, Griffiths KL, Lam WY, Gopal R, Kang DD, Ahmed M, Rajamanickam A, Cruz-Lagunas A, Zuniga J, Babu S, et al. (2015). Helminth-induced arginase-1 exacerbates lung inflammation and disease severity in tuberculosis. J Clin Invest 125, 4699–4713. [PubMed: 26571397]

Moriyama S, and Artis D (2019). Neuronal regulation of group 2 innate lymphoid cells and type 2 inflammation. Adv Immunol 143, 1–9. [PubMed: 31607366]

Muller PA, Matheis F, and Mucida D (2020). Gut macrophages: key players in intestinal immunity and tissue physiology. Curr Opin Immunol 62, 54–61. [PubMed: 31841704]

Nadjsombati MS, McGinty JW, Lyons-Cohen MR, Jaffe JB, DiPeso L, Schneider C, Miller CN, Pollack JL, Nagana Gowda GA, Fontana MF, et al. (2018). Detection of Succinate by Intestinal

Tuft Cells Triggers a Type 2 Innate Immune Circuit. Immunity 49, 33–41 e37. [PubMed: 30021144]

Nayak DP, and Kelley GW (1965). Synergistic Effect of Ascaris Migration and Influenza Infection in Mice. J Parasitol 51, 297–298. [PubMed: 14275227]

Ogilvy S, Elefanty AG, Visvader J, Bath ML, Harris AW, and Adams JM (1998). Transcriptional regulation of vav, a gene expressed throughout the hematopoietic compartment. Blood 91, 419–430. [PubMed: 9427694]

Oliphant CJ, Hwang YY, Walker JA, Salimi M, Wong SH, Brewer JM, Englezakis A, Barlow JL, Hams E, Scanlon ST, et al. (2014). MHCII-mediated dialog between group 2 innate lymphoid cells and CD4(+) T cells potentiates type 2 immunity and promotes parasitic helminth expulsion. Immunity 41, 283–295. [PubMed: 25088770]

Osborne LC, Monticelli LA, Nice TJ, Sutherland TE, Siracusa MC, Hepworth MR, Tomov VT, Kobuley D, Tran SV, Bittinger K, et al. (2014). Coinfection. Virus-helminth coinfection reveals a microbiota-independent mechanism of immunomodulation. Science 345, 578–582. [PubMed: 25082704]

Perez OA, Yeung ST, Vera-Licona P, Romagnoli PA, Samji T, Ural BB, Maher L, Tanaka M, and Khanna KM (2017). CD169(+) macrophages orchestrate innate immune responses by regulating bacterial localization in the spleen. Sci Immunol 2.

Purtha WE, Myers N, Mitaksov V, Sitati E, Connolly J, Fremont DH, Hansen TH, and Diamond MS (2007). Antigen-specific cytotoxic T lymphocytes protect against lethal West Nile virus encephalitis. Eur J Immunol 37, 1845–1854. [PubMed: 17559174]

Reese TA, Wakeman BS, Choi HS, Hufford MM, Huang SC, Zhang X, Buck MD, Jezewski A, Kambal A, Liu CY, et al. (2014). Helminth infection reactivates latent gammaherpesvirus via cytokine competition at a viral promoter. Science 345, 573–577. [PubMed: 24968940]

Reynolds LA, Filbey KJ, and Maizels RM (2012). Immunity to the model intestinal helminth parasite Heligmosomoides polygyrus. Semin Immunopathol 34, 829–846. [PubMed: 23053394]

Rolot M, Dougall AM, Chetty A, Javaux J, Chen T, Xiao X, Machiels B, Selkirk ME, Maizels RM, Hokke C, et al. (2018). Helminth-induced IL-4 expands bystander memory CD8(+) T cells for early control of viral infection. Nat Commun 9, 4516. [PubMed: 30375396]

Salgame P, Yap GS, and Gause WC (2013). Effect of helminth-induced immunity on infections with microbial pathogens. Nat Immunol 14, 1118–1126. [PubMed: 24145791]

Scheer S, Krempl C, Kallfass C, Frey S, Jakob T, Mouahid G, Mone H, Schmitt-Graff A, Staeheli P, and Lamers MC (2014). S. mansoni bolsters anti-viral immunity in the murine respiratory tract. PLoS One 9, e112469. [PubMed: 25398130]

Schneider C, O'Leary CE, von Moltke J, Liang HE, Ang QY, Turnbaugh PJ, Radhakrishnan S, Pellizzon M, Ma A, and Locksley RM (2018). A Metabolite-Triggered Tuft Cell-ILC2 Circuit Drives Small Intestinal Remodeling. Cell 174, 271–284 e214. [PubMed: 29887373]

Shi J, Hua L, Harmer D, Li P, and Ren G (2018). Cre Driver Mice Targeting Macrophages. Methods Mol Biol 1784, 263–275. [PubMed: 29761406]

Shrestha B, and Diamond MS (2004). Role of CD8+ T cells in control of West Nile virus infection. J Virol 78, 8312–8321. [PubMed: 15254203]

Sivagnanam M, Mueller JL, Lee H, Chen Z, Nelson SF, Turner D, Zlotkin SH, Pencharz PB, Ngan BY, Libiger O, et al. (2008). Identification of EpCAM as the gene for congenital tufting enteropathy. Gastroenterology 135, 429–437. [PubMed: 18572020]

Stanley D, Mason LJ, Mackin KE, Srikhanta YN, Lyras D, Prakash MD, Nurgali K, Venegas A, Hill MD, Moore RJ, et al. (2016). Translocation and dissemination of commensal bacteria in post-stroke infection. Nat Med 22, 1277–1284. [PubMed: 27694934]

Straub T, Freudenberg MA, Schleicher U, Bogdan C, Gasteiger G, and Pircher H (2018). Bacterial coinfection restrains antiviral CD8 T-cell response via LPS-induced inhibitory NK cells. Nat Commun 9, 4117. [PubMed: 30297690]

Sule WF, Oluwayelu DO, Hernandez-Triana LM, Fooks AR, Venter M, and Johnson N (2018). Epidemiology and ecology of West Nile virus in sub-Saharan Africa. Parasit Vectors 11, 414. [PubMed: 30005653]

Szabo R, Callies LK, and Bugge TH (2019). Matriptase drives early-onset intestinal failure in a mouse model of congenital tufting enteropathy. Development 146.

Thackray LB, Handley SA, Gorman MJ, Poddar S, Bagadia P, Briseno CG, Theisen DJ, Tan Q, Hykes BL Jr., Lin H, et al. (2018). Oral Antibiotic Treatment of Mice Exacerbates the Disease Severity of Multiple Flavivirus Infections. Cell Rep 22, 3440–3453 e3446. [PubMed: 29590614]

Ting HA, and von Moltke J (2019). The Immune Function of Tuft Cells at Gut Mucosal Surfaces and Beyond. J Immunol 202, 1321–1329. [PubMed: 30782851]

Urban JF Jr., Noben-Trauth N, Donaldson DD, Madden KB, Morris SC, Collins M, and Finkelman FD (1998). IL-13, IL-4Ralpha, and Stat6 are required for the expulsion of the gastrointestinal nematode parasite Nippostrongylus brasiliensis. Immunity 8, 255–264. [PubMed: 9492006]

Urban JF Jr., Schopf L, Morris SC, Orekhova T, Madden KB, Betts CJ, Gamble HR, Byrd C, Donaldson D, Else K, et al. (2000). Stat6 signaling promotes protective immunity against Trichinella spiralis through a mast cell- and T cell-dependent mechanism. J Immunol 164, 2046–2052. [PubMed: 10657657]

VanBlargan LA, Himansu S, Foreman BM, Ebel GD, Pierson TC, and Diamond MS (2018). An mRNA Vaccine Protects Mice against Multiple Tick-Transmitted Flavivirus Infections. Cell Rep 25, 3382–3392.e3383. [PubMed: 30566864]

Vergnolle N, and Cirillo C (2018). Neurons and Glia in the Enteric Nervous System and Epithelial Barrier Function. Physiology (Bethesda) 33, 269–280. [PubMed: 29897300]

von Moltke J, Ji M, Liang HE, and Locksley RM (2016). Tuft-cell-derived IL-25 regulates an intestinal ILC2-epithelial response circuit. Nature 529, 221–225. [PubMed: 26675736]

Wescott RB, and Todd AC (1966). Interaction of Nippostrongylus Brasiliensis and Influenza Virus in Mice .I. Influence of Nematode on Virus. Journal of Parasitology 52, 242-&.

White JP, Xiong S, Malvin NP, Khoury-Hanold W, Heuckeroth RO, Stappenbeck TS, and Diamond MS (2018). Intestinal Dysmotility Syndromes following Systemic Infection by Flaviviruses. Cell 175, 1198–1212 e1112. [PubMed: 30293866]

Wilen CB, Lee S, Hsieh LL, Orchard RC, Desai C, Hykes BL Jr., McAllaster MR, Balce DR, Feehley T, Brestoff JR, et al. (2018). Tropism for tuft cells determines immune promotion of norovirus pathogenesis. Science 360, 204–208. [PubMed: 29650672]

Zhu J, Guo L, Watson CJ, Hu-Li J, and Paul WE (2001). Stat6 is necessary and sufficient for IL-4's role in Th2 differentiation and cell expansion. J Immunol 166, 7276–7281. [PubMed: 11390477]

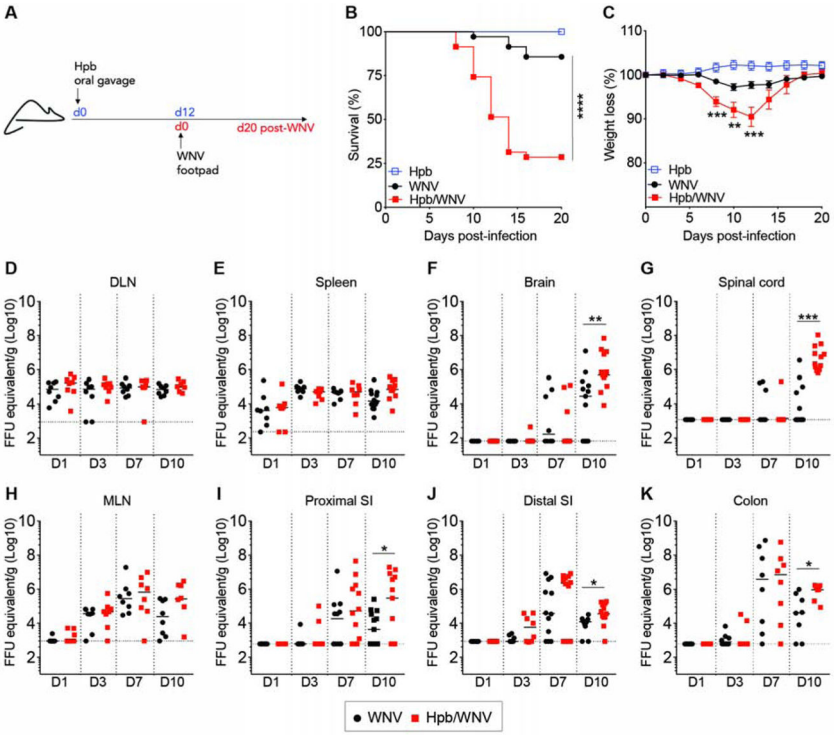

Figure 1. Coinfection with enteric helminths enhances susceptibility to WNV.

(**A**) Experimental scheme of Hpb and WNV coinfection of C57BL6/J mice. (**B**) Mortality was measured after WNV infection (log-rank test with Bonferroni correction: **** $P <$ 0.0001; 4 experiments, n = 30 to 35 per group. (**C**) Weight loss measurements (one-way ANOVA with Holm-Sidak's post-test; statistical comparison is for WNV-infected and coinfected mice: ** $P < 0.01$, *** $P < 0.001$; 3 experiments, n = 14 to 25 per group. (**D-K**) WNV RNA levels in (**D**) inguinal lymph nodes [DLN], (**E**) spleen, (**F**) brain, (**G**) spinal cord, (**H**) mesenteric lymph nodes [MLN], (**I**) proximal SI, (**J**) distal SI, and (**K**) colon (n = 8 to 12 mice per group, 2 to 3 experiments) Mann-Whitney test: * $P < 0.05$, ** $P < 0.01$, *** $P < 0.001$). Bars, median values; Dotted lines, limit of detection (LOD). **See also** Fig S1.

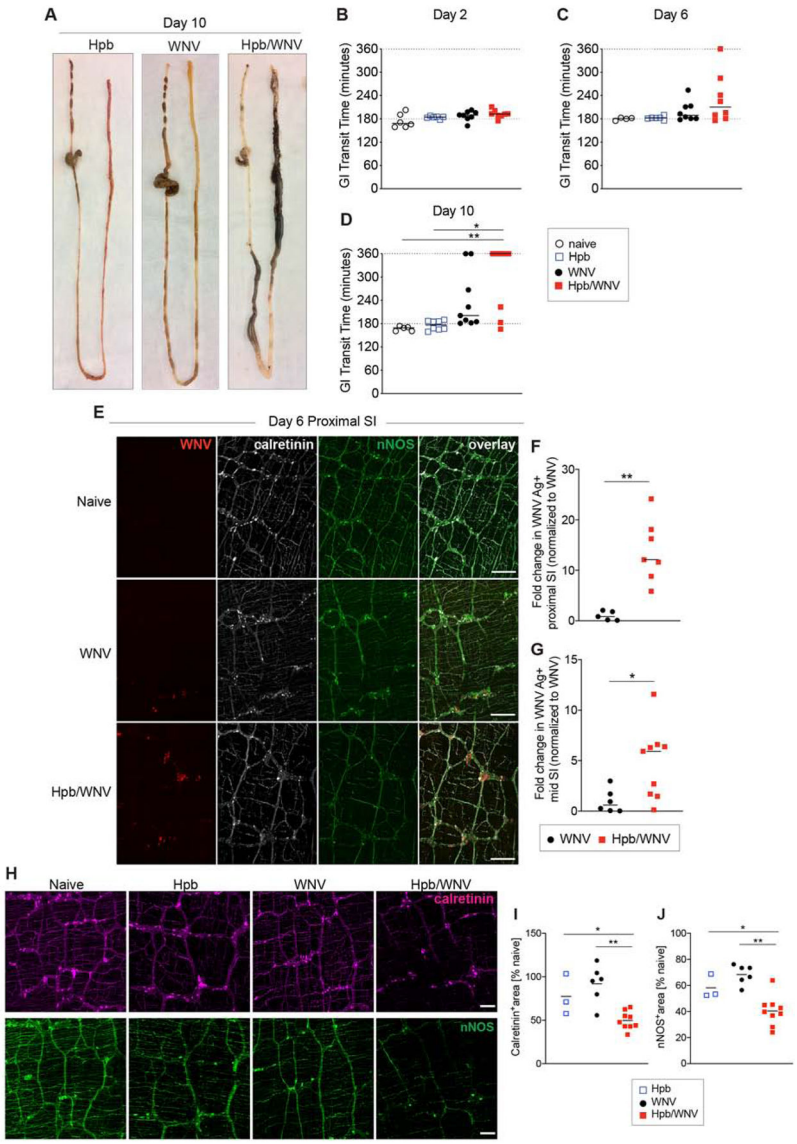

Figure 2. Coinfection causes changes in the GI tract that exacerbate intestinal motility defects.

(**A**) Intestines were isolated at 10 days after WNV infection or 22 days after Hpb infection (representative of 4 experiments). (**B-D**) GI tract transit time of different infection cohorts (at 2 (**B**), 6 (**C**), or 10 (**D**) days after WNV-infection) after gavage of carmine red dye (3 experiments; n = 8 to 12 mice per group). (**E**) Muscularis propria from the proximal SI of naïve, WNV-infected and coinfected mice (6 dpi) was stained for WNV antigen (red), calretinin (white) and nNOS (green). (**F-G**) WNV antigen staining was quantified, and the coinfected group is represented as fold-change compared to proximal SI (**F**) and mid SI (**G**) sections from WNV-only infected mice (2 experiments; n = 5 to 9 mice per group). Scale bar: 200 μm. (**H-J**) Muscularis propria from the proximal SI of indicated groups stained for calretinin (magenta) and nNOS (green). Expression was quantified as percent positive area compared to preparations from naïve mice. Scale bar: 100 μm. Images are representative. Data are from 2 experiments; n = 3 to 9 mice per group. **B-D**. Kruskal-Wallis ANOVA with Dunn's post-test. **F-G and I-J**. Mann-Whitney test. * $P < 0.05$, ** $P < 0.01$. **See also** Fig S2.

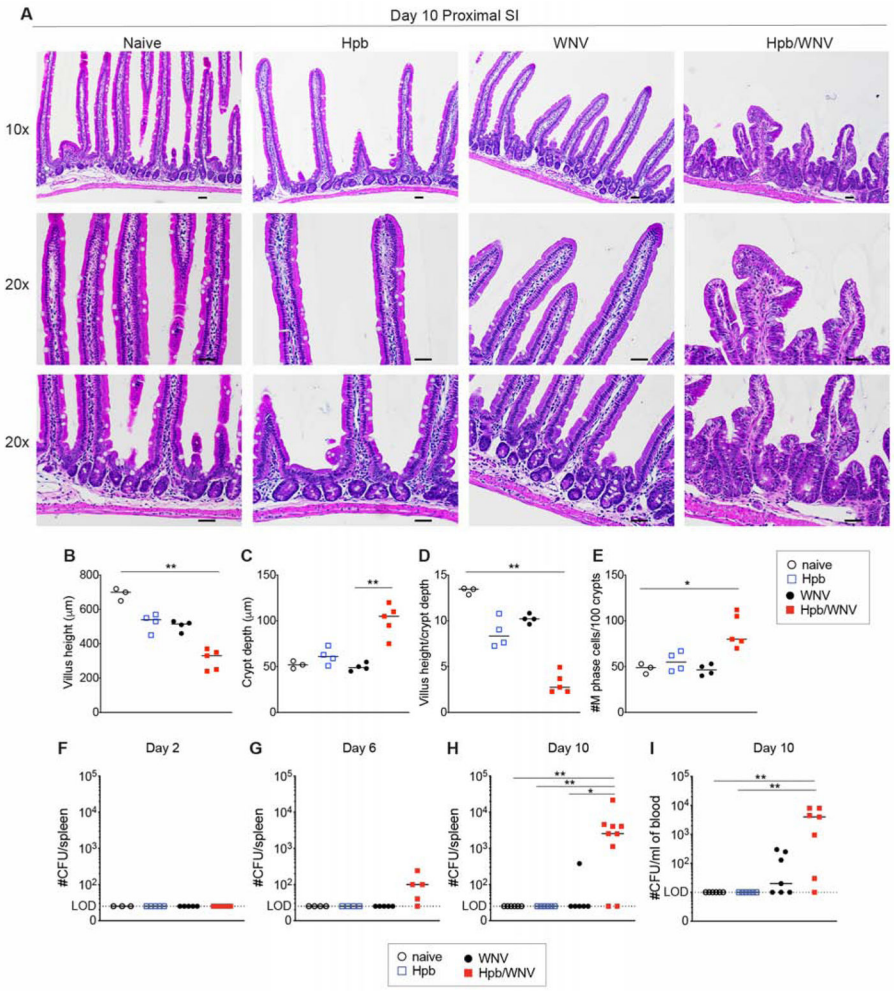

Figure 3. Hpb and WNV coinfection causes changes in the intestinal mucosa that enable translocation of commensal bacteria.

(**A-E**) Proximal SI sections from indicated groups were isolated at 10 dpi with WNV or 22 days after Hpb infection and stained with hematoxylin and eosin. Scale bar: 50 μm. Two experiments with n = 3 to 5 mice per group. (**B-D**) Villus height and crypt depth was measured (50 per group) in the proximal SI, and the ratio was quantified. (**E**) M phase cells in crypts were counted (200 crypts per group) in the proximal SI. Two experiments with n = 3 to 5 mice in per group. (**F-I**) Homogenized spleens (**F-H**) or blood (**I**) from different groups at indicated time points (2 (**F**), 6 (**G**), or 10 (**H-I**) dpi) was added to blood-agar plates. Bacterial colony counts were enumerated (2 to 3 experiments; n = 3 to 9 mice per group). **B-I**: Kruskal-Wallis ANOVA with Dunn's post-test; * $P < 0.05$, ** $P < 0.01$). Bars. median values; Dotted line, LOD. **See also** Fig S3.

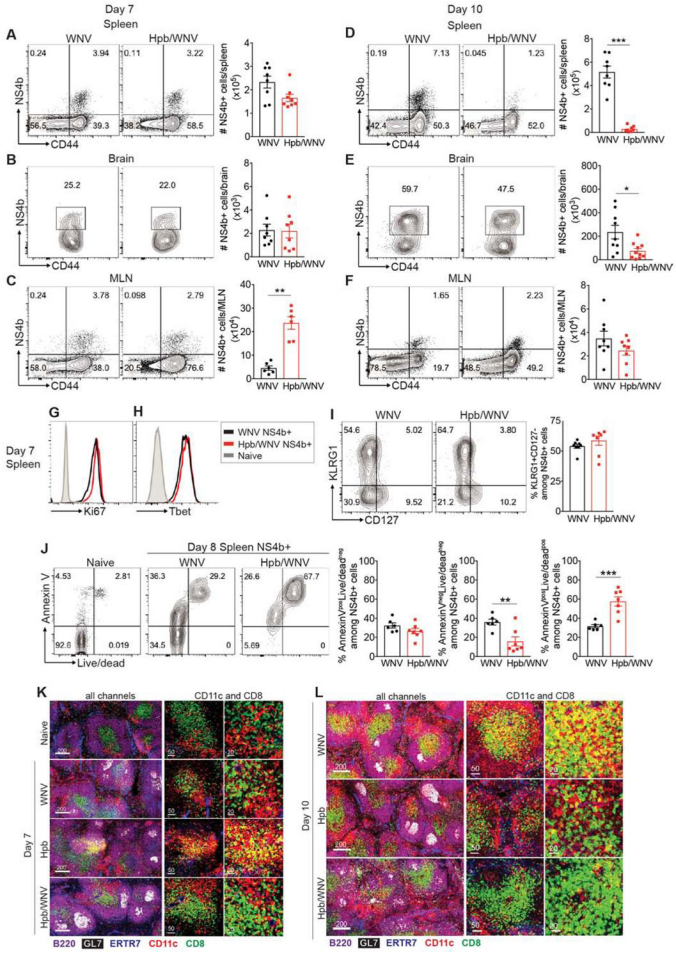

Figure 4. Coinfected mice show a collapse in WNV-specific CD8$^+$ T cell responses.

C57BL/6J mice were infected with WNV or coinfected with Hpb and WNV. (**A-C**) At 7 or (**D-F**) 10 dpi, spleens, brains, and MLNs were stained with antibodies to CD45, CD3, CD8, and CD44, and WNV NS4B D^b-restricted tetramers and gated on CD45$^+$CD3$^+$CD8$^+$ cells. NS4B-positive cells are quantified besides each plot (2 to 3 experiments, n = 8 mice per group). (**G-J**) At 7 dpi, splenocytes also were stained for (**G, H**) Ki67 and T-bet or (**I**) KLRG1 and CD127 (2 experiments, n = 6 to 8 mice per group). (**J**) Spleens from indicated groups were harvested at 8 dpi and stained for Annexin V in addition to T cell markers and NS4B tetramers. The percentages of Annexin V versus live/dead cell subsets were compared (2 experiments; n = 6 to 8 mice per group). (**K-L**) Spleen sections harvested from different groups at 7 (**K**) or 10 (**L**) dpi were stained with antibodies against B220, GL7, ERTR7, CD11c and CD8. Two experiments with n = 3 to 4 mice per group. **C-E and J:** unpaired t test: ** $P < 0.01$, *** $P < 0.001$. **See also** Fig S4 and S8.

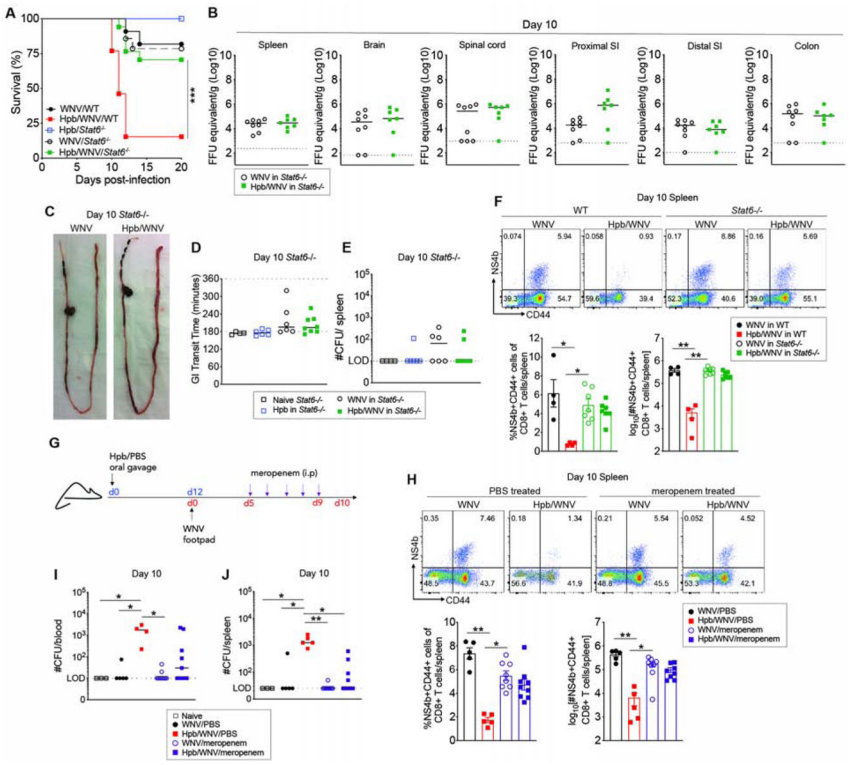

Figure 5. A Stat6 deficiency rescues coinfected mice from gut-associated phenotypes.

WT and *Stat6*$^{-/-}$ mice were infected with Hpb or WNV or coinfected with Hpb and WNV. (**A**) Survival analysis from 3 experiments (log-rank test with Bonferroni correction: *** $P <$ 0.001; n = 8 to 15 per group). (**B**) Tissues viral RNA levels at 10 dpi (2 to 3 experiments; n = 7 to 8 mice per group; Mann-Whitney test: no differences observed). (**C**) Intestines from *Stat6*$^{-/-}$ mice infected with WNV or coinfected at 10 dpi. (**D**) GI tract transit time in *Stat6*$^{-/-}$ mice at indicated time points (2 experiments; n = 4 to 8 mice per group. (**E**) Splenic homogenates from *Stat6*$^{-/-}$ were harvested and bacterial colony counts were quantified (2 experiments; n = 4 to 8 mice per group. (**F**) Splenocytes from WNV-infected or coinfected mice from WT and *Stat6*$^{-/-}$ mice were stained with antibodies to CD45, CD3, CD8, and CD44, and WNV NS4B D^b-restricted tetramers (2 experiments; gated on $CD45^+CD3^+CD8^+$ T cells; n = 4 to 8 mice per group. (**G**) Experimental scheme of mice receiving PBS or meropenem (500 μg) twice daily starting from day 5 post-WNV infection until day 9. (**H**) Splenocytes from WNV-infected or coinfected mice treated with meropenem or PBS were stained for WNV-specific $CD8^+$ T cells as described in panel **F** (2 experiments; n = 5 to 9 mice per group). (**I**) Blood and (**J**) splenic homogenates from naïve, singly-infected, or coinfected WT mice treated with meropenem or PBS were harvested at 10 dpi, and the bacterial colony count was quantified (2 experiments; n = 3 to 9 mice per group). **D-F and H-J**: Kruskal-Wallis ANOVA with Dunn's post-test: panels **D-E**: not significant; panels **F, H-J**: * $P < 0.05$; ** $P < 0.01$). **See also** Fig S5 and S8.

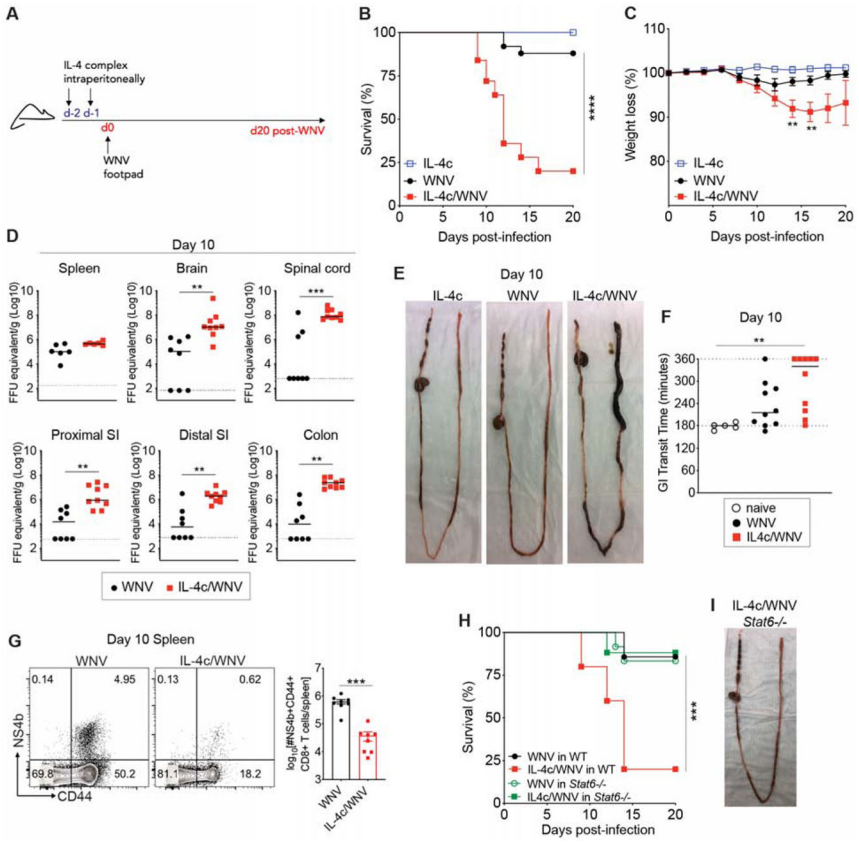

Figure 6. Treatment of WNV-infected mice with IL-4c.

(**A**) Groups of WT mice were treated with IL-4c or PBS on two consecutive days prior to WNV infection, and (**B**) survival and (**C**) weight loss were determined (**B**: 3 experiments; n = 10 to 25 per group; **C**: 2 experiments; significance is shown for WNV-infected and IL-4c/WNV comparison: n = 5 to 15 per group). (**D**) Indicated tissues were harvested at 10 dpi, and WNV RNA was measured (2 experiments, n = 6 to 8 mice per group). Dotted lines, LOD. (**E**) Intestines were isolated at 10 dpi (representative of 3 experiments). (**F**) GI tract transit time was measured at indicated time points (2 experiments; n = 5 to 12 mice per group). (**G**) Splenocytes were stained with antibodies to CD45, CD3, CD8, CD44, and WNV NS4B D^b-restricted tetramers (2 experiments; gated on $CD45^+CD3^+CD8^+$ T cells; n = 6 to 8 mice per group). (**H**) WT and *Stat6*$^{-/-}$ mice were treated with IL-4c, inoculated with WNV, and monitored for survival (2 experiments; n = 10 to 15 per group). (**I**) Intestines from *Stat6*$^{-/-}$ mice treated with IL-4c and WNV. **B and I**: log-rank test with Bonferroni correction. **C**: one-way ANOVA with Holm-Sidak's post-test. **D**. Mann-Whitney test. **E**. Kruskal-Wallis ANOVA with Dunn's post-test. **G**. Unpaired t test (** $P < 0.01$, *** $P < 0.001$: **** $P < 0.0001$). **See also** Fig S6 and S8.

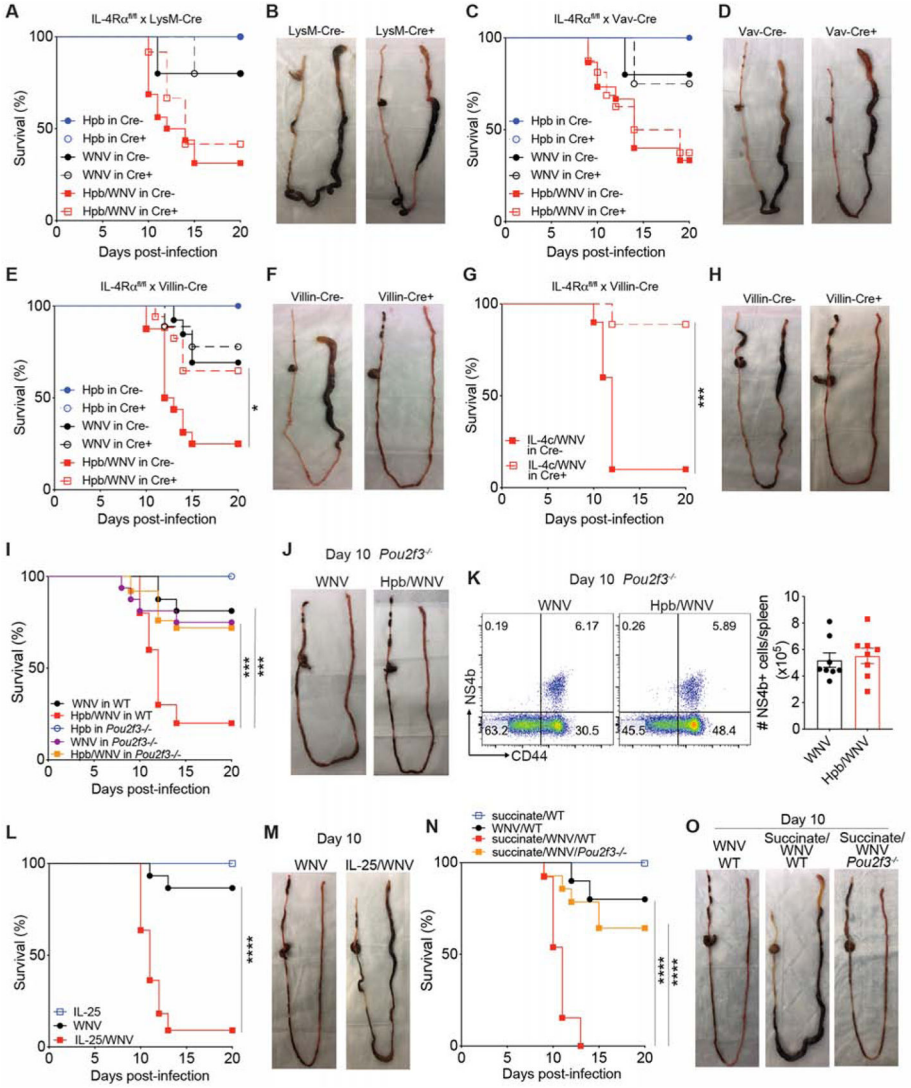

Figure 7. Coinfection-induced mortality depends on intestinal epithelial cell expression of IL-4Rα and tuft cells

(**A**) Mice lacking IL-4Rα expression on myeloid cells [LysM Cre^{+} IL-4Rα$^{fl/fl}$] and [Cre^{-} IL-4Rα$^{fl/fl}$] littermate controls were singly or coinfected and evaluated for survival. (**B**) Intestines from LysM Cre^{+} IL-4Rα$^{fl/fl}$ mice and Cre^{-} IL-4Rα$^{fl/fl}$ controls were isolated at 10 dpi. Mice lacking IL-4Rα on hematopoietic cells [Vav Cre^{+} IL-4Rα$^{fl/fl}$] and [Cre^{-} IL-4Rα$^{fl/fl}$] littermate controls were examined for (**C**) survival and (**D**) gut pathology. Mice lacking IL-4Rα on intestinal epithelial cells [Villin Cre^{+} IL-4Rα$^{fl/fl}$] and [Cre^{-} IL-4Rα$^{fl/fl}$] littermate controls were examined for (**E**) mortality and (**F**) gut pathology. Mice lacking IL-4Rα on intestinal epithelial cells and littermate controls were treated with IL-4c (i.p.) prior to WNV infection and (**G**) mortality was monitored. (**H**) Intestines from mice in (**G**) were isolated at 10 dpi. **A, C, E, G**: 2 to 3 experiments; n = 5 to 15 per group. (**B, D, F, H**) Images from two experiments (n = 8 mice per group). (**I**) WT or *Pou2f3*$^{-/-}$ mice were singly or coinfected and monitored (3 experiments, n = 8 to 25 per group). (**J**) Intestines from *Pou2f3*$^{-/-}$ mice infected with WNV or Hpb and WNV were isolated at 10 dpi. Three

experiments (n = 10). (**K**) Splenocytes isolated at 10 dpi from WNV-infected and coinfected *Pou2f3*$^{-/-}$ mice stained for WNV-specific CD8^{+} T cells as indicated in Fig 4 (2 experiments; n = 8). (**L-M**) WT mice were treated with IL-25 or PBS for two consecutive days prior to WNV infection and (**L**) monitored for survival. (**M**) Intestines from WNV-infected and IL-25/WNV treated mice were isolated at 10 dpi. (**N-O**) WT or *Pou2f3*$^{-/-}$ mice were supplemented with succinate in drinking water 7 days prior to WNV infection and (**N**) monitored for survival. (**O**) Intestines from WNV-only infected and succinate-treated and WNV-infected mice were isolated at 10 dpi. (**L and N**) 2 experiments: (**L**) n = 5 to 15 per group; (**N**) n = 5 to 14 per group. **A, C, E, G, I, L, N**: log-rank test with Bonferroni correction (* $P < 0.05$, *** $P < 0.001$; **** $P < 0.0001$. **K**: unpaired t test; no statistical differences observed). **See also** Fig S7 and S8.